Biomedicine & Pharmacotherapy 144 (2021) 112255

Contents lists available at ScienceDirect

Biomedicine & Pharmacotherapy

journal homepage: www.elsevier.com/locate/biopha

The natural product vioprolide A exerts anti-inflammatory actions through inhibition of its cellular target NOP14 and downregulation of importin-dependent NF-κB p65 nuclear translocation

Luisa D. Burgers [a], Betty Luong [a], Yanfen Li [c], Matthias P. Fabritius [d,e], Stylianos Michalakis [c], Christoph A. Reichel [d], Rolf Müller [f], Robert Fürst [a,b,*]

[a] Institute of Pharmaceutical Biology, Faculty of Biochemistry, Chemistry and Pharmacy, Goethe University, Frankfurt, Germany
[b] LOEWE Center for Translational Biodiversity Genomics (LOEWE-TBG), Frankfurt, Germany
[c] Department of Ophthalmology, University Hospital, LMU Munich, Munich, Germany
[d] Department of Otorhinolaryngology and Walter Brendel Centre of Experimental Medicine, Clinical Centre of LMU Munich, Munich, Germany
[e] Department of Radiology, University Hospital, LMU Munich, Munich, Germany
[f] Department of Microbial Natural Products, Helmholtz-Institute for Pharmaceutical Research Saarland, Helmholtz Center for Infection Research and Department of Pharmacy at Saarland University, Saarbrücken, Germany

ARTICLE INFO

Keywords:
Vioprolide A
Natural product
Endothelial cells
Inflammation
Protein synthesis
Nucleolar protein 14

ABSTRACT

Chronic inflammation is characterized by persisting leukocyte infiltration of the affected tissue, which is enabled by activated endothelial cells (ECs). Chronic inflammatory diseases remain a major pharmacotherapeutic challenge, and thus the search for novel drugs and drug targets is an ongoing demand. We have identified the natural product vioprolide A (vioA) to exert anti-inflammatory actions *in vivo* and in ECs *in vitro* through inhibition of its cellular target nucleolar protein 14 (NOP14). VioA attenuated the infiltration of microglia and macrophages during laser-induced murine choroidal neovascularization and the leukocyte trafficking through the vascular endothelium in the murine cremaster muscle. Mechanistic studies revealed that vioA downregulates EC adhesion molecules and the tumor necrosis factor receptor (TNFR) 1 by decreasing the *de novo* protein synthesis in ECs. Most importantly, we found that inhibition of importin-dependent NF-κB p65 nuclear translocation is a crucial part of the action of vioA leading to reduced NF-κB promotor activity and inflammatory gene expression. Knockdown experiments revealed a causal link between the cellular target NOP14 and the anti-inflammatory action of vioA, classifying the natural product as unique drug lead for anti-inflammatory therapeutics.

1. Introduction

In the field of drug discovery, natural products constitute an ample amount of structurally diverse biomolecules, which have evolutionary evolved and target distinct, in part unexplored molecular pathways. Such natural products have been found in a broad range of organisms, including bacteria, plants, marine species and myxobacteria.

In the present study, we introduce the natural product vioprolide A (vioA), a secondary metabolite isolated from the myxobacterium *Cystobacter violaceus*, as anti-inflammatory compound. The molecular structure of vioA contains a trans-(2*S*,4*R*)-4-methylazetidinecarboxylic acid, which has not been described for any other natural product before [1]. Studies on this secondary metabolite are rare. However, it was shown that vioA increases the caspase-8-dependent production of IL-1β in macrophages (concentrations of 0.1–20 μM) and induces apoptosis in cancer cells (concentrations of 5–50 nM) [2,3].

Abbreviations: CAM, cell adhesion molecule; CNV, choroidal neovascularization; EGTA, ethylene glycol-bis(β-aminoethyl ether)-N,N,N',N'-tetraacetic acid; HUVEC, human umbilical vein endothelial cell; ICAM-1, intercellular adhesion molecule 1; IKK, nuclear factor of kappa light polypeptide gene enhancer in B-cells inhibitor alpha kinase; IκBα, nuclear factor of kappa light polypeptide gene enhancer in B-cells inhibitor alpha; KPNA2, karyopherin alpha 2; KPNA4, karyopherin alpha 4; KPNB1, karyopherin beta 1; NF-κB, nuclear factor 'kappa-light-chain-enhancer' of activated B-cells; NOP14, nucleolar protein 14; PBMC, primary blood mononuclear cell; PL, primary lymphocyte; RIPA, radioimmunoprecipitation assay; SDF-1, stromal-cell derived factor 1; TAK, TGF-β-activated kinase; TNF, tumor necrosis factor; TNFR1, tumor necrosis factor receptor 1; VCAM-1, vascular endothelial cell adhesion molecule 1; VioA, vioprolide A.

* Correspondence to: Institute of Pharmaceutical Biology, Goethe University Frankfurt, Max-von-Laue-Str. 9, 60438 Frankfurt, Germany.
E-mail address: fuerst@em.uni-frankfurt.de (R. Fürst).

https://doi.org/10.1016/j.biopha.2021.112255
Received 5 July 2021; Received in revised form 18 September 2021; Accepted 26 September 2021
Available online 2 October 2021

Recently, the nucleolar protein 14 (NOP14) has been identified as cellular target of vioA. NOP14 takes part in the ribosomal biogenesis as well as formation of the small subunit processome [3]. Various studies, which have been conducted over the past years, underline the involvement of NOP14 in angiogenic processes in cancer [4–7]. Interestingly, however, nothing is known about the general involvement of NOP14 in inflammatory actions. Thus, investigations concerning the relevance of NOP14 regarding crucial cellular processes are of high interest.

Inflammation is a complex biological process that protects the body against infections and injuries [8]. In this context, the vascular endothelium creates a barrier between the blood and the tissue, thereby controlling the extravasation of serum proteins and leukocytes towards the origin of inflammation [9–11]. Upon induction of an inflammatory response, inflammatory cytokines like tumor necrosis factor (TNF) activate endothelial cells through ligand-receptor binding and initiate downstream signaling pathways, including the NF-κB cascade [12,13]. In a normal state, NF-κB subunits, such as RELA (also known as p65), are retained in the cytosol by masking of their nuclear localization sequence (NLS) through the inhibitory protein IκBα. Upon phosphorylation and degradation of IκBα, the NF-κB subunits are released and transported into the nucleus through the classical nuclear import pathway. Thereby a trimeric complex is established with both a carrier protein of the importin α-family, which binds the NLS of the NF-κB subunit, and the importin β-family, which interacts with the nuclear pore complex [14]. Multiple studies indicate an important role of importin subunit alpha-1, importin subunit alpha-3 and importin subunit beta-1 during the nuclear import of the NF-κB subunit p65 [15–20]. In the nucleus, NF-κB acts as transcription factor by binding to the promotor region of proinflammatory genes, amongst them the CAM encoding genes *ICAM1*, *VCAM1*, and *SELE* [21]. CAMs promote the rolling and firm adherence of leukocytes to the endothelium.

Physiologically, the inflammatory response is resolved, and the tissue is restored [22]. However, through failing eradication or constant cytokine stimulation, the inflammatory response can become chronic, which is classified by a deregulated endothelial barrier function coupled with the exaggerated and ongoing leukocyte infiltration into the tissue [23]. This is observed in multiple chronic diseases, including atherosclerosis and rheumatoid arthritis [24,25]. Given its important role in chronic inflammation, the vascular endothelium thus represents an interesting therapeutic target for treating inflammation-based diseases.

In our study, we highlight the potent and advantageous actions of the natural product vioA on inflammation-related actions in human vascular endothelial cells *in vivo* and *in vitro*. Moreover, we show for the first time, that inhibition of the nucleolar protein 14, the cellular target of vioA, evokes anti-inflammatory effects on the TNF-activated human vascular endothelium.

2. Materials and methods

2.1. Compounds

Vioprolide A was kindly provided by the group of Prof. Dr. Rolf Müller (Helmholtz Institute for Pharmaceutical Research Saarland, Saarland University, Saarland, Germany) and was dissolved in dimethyl sulfoxide (DMSO, Sigma-Aldrich, St. Louis, MO, USA) to obtain a stock solution of 1 mM and stored at −80 °C. Cycloheximide (CHX) was purchased from Sigma-Aldrich, dissolved in DMSO to a stock solution of 100 mg/ml and stored at −20 °C. For cell culture purposes, the stock solutions were freshly diluted using cell culture medium without exceeding a final DMSO concentration of 0.01% (v/v). Human tumor necrosis factor (TNF) and stromal-cell derived factor 1 (SDF-1) were purchased from PeproTech (Rocky Hill, NJ, USA).

2.2. Cell culture

HUVECs were isolated from human umbilical veins as previously described [26]. Briefly, human umbilical veins were flushed with PBS containing Ca^{2+} and Mg^{2+} and treated with collagenase A (0.1 g/L; Roche, Basel, Switzerland) for 45 min to detach the cells. Detachment reaction was stopped using medium 199 (M199, PAN-Biotech, Aidenbach, Germany) supplemented with 10% fetal calf serum (FCS, Biochrom, Berlin, Germany), 100 U/ml penicillin and 100 μg/ml streptomycin (PAN-Biotech). The collected, HUVECs-containing M199 was centrifuged at 300 g for 5 min. The supernatant was discarded, and the cell pellet was resuspended in endothelial cell growth medium (EASY ECGM, PELOBiotech, Planegg/Martinsried, Germany) containing 10% FCS (Biochrom), 100 U/ml penicillin, 100 μg/ml streptomycin (PAN-Biotech), 2.5 μg/ml amphotericin B (PAN-Biotech) and a supplement mixture (PELOBiotech). Cells were grown on collagen G (10 μg/ml; Biochrom, Berlin, Germany)-coated 25 cm^2 flasks under constant humidity in an atmosphere of 5% CO_2 and 37 °C. HUVECs were cultivated to passage 2 and used for experimental purposes in passage 3. THP-1 cells and Jurkat cells were obtained from the Germany collection of Microorganisms and Cell Cultures (DSMZ, Braunschweig, Germany; THP-1: DSMZ no. ACC-16; Jurkat: DSMZ no. ACC-282) and cultivated in Royal Park Memorial Institute 1640 (RPMI; PAN-Biotech) supplemented with 10% FCS (Biochrom), 100 U/ml penicillin and 100 μg/ml streptomycin (PAN-Biotech). For experimental purposes, THP-1 cells and Jurkat cells were used up to passage 30.

2.3. Isolation of human PLs and PBMCs

PLs and PBMCs were isolated from buffy coats obtained from Deutsches Rotes Kreuz, Blutspendedienst Baden-Württemberg/Hessen, Institut für Transfusionsmedizin und Immunhämatologie, Frankfurt, Germany following the instructions of Bøyum [27]. In brief, plasma cells were separated by low density gradient centrifugation using lymphocyte separation medium (PromoCell, Heidelberg, Germany). For obtaining PLs, PBMCs were resuspended in RPMI supplemented with 10% FCS (Biochrom), 100 U/ml penicillin and 100 μg/ml streptomycin (PAN--Biotech), added to 6-well plates (Sarstedt, Nürnberg, Germany) and allowed to adhere for 90 min. Unattached PLs were separated from attached monocytes and cultivated for 24 h in RPMI containing 10% FCS (Biochrom), 100 U/ml penicillin and 100 μg/ml streptomycin (PAN--Biotech) before they were used for cell adhesion assays. PBMCs were used for cell adhesion assays directly after being isolated.

2.4. Animals

For the *in vivo* laser-induced choroidal neovascularization (CNV) experiment, 6–8-week-old female C57BL/6 J WT mice (Charles River Laboratories, Wilmington, MA, USA) were used and for the *in vivo* intravital microscopy of the murine cremaster muscle 10–20 weeks old male C57BL/6 mice (Charles River Laboratories, Sulzfeld, Germany) were used. Animals were housed on a 12–h light/dark cycle with free access to water and food.

2.5. Laser-induced choroidal neovascularization

To induce choroidal neovascularization in mice, laser coagulation was used as described [28]. Briefly, mice were anesthetized by an intraperitoneal injection of a mixture of ketamine (40 mg/kg body weight) and xylazine (20 mg/kg body weight), and their pupils were dilated with tropicamide (Mydriadicum Stulln, Pharma Stulln GmbH). For vioprolide A administration, 1 μl of vioprolide A was intravitreally delivered into right eyes and 1 μl of vehicle was applied to left eyes as control. CNV was induced by laser photocoagulation immediately after intravitreal injection. Retinal fundus was visualized with Micron IV Retinal Imaging Microscope (Phoenix Research Laboratories) and laser burns were induced with an image-guided laser system (Phoenix Research Laboratories). Four laser burns with 532 nm argon laser (230 mW, 70 ms duration) were applied to each eye to disrupt the Bruch's

membrane.

Mice were euthanatized 14 days after CNV. Eyes were enucleated and eyecup were isolated from the posterior area of the eye. They were flat-mounted and fixed in 4% paraformaldehyde for immunohistochemistry studies. Flat-mounts were immunostained with rabbit anti-Iba1 (1:500, Wako, 019–19741) and Alexa Fluor 488-conjugated *Griffonia simplicifolia* isolectin B4 (IB4, 1:25, Thermo Fisher Scientific, I21411), and then followed by the incubation in presence of secondary antibody Alexa Fluor 555 donkey anti-rabbit IgG (1:500, Invitrogen, A-31572).

The flat mounts were viewed under Leica TCS SP8 spectral confocal laser scanning microscope (Leica, Wetzlar, Germany). Images were captured with identical settings and the accumulation of $Iba1^+$ microglia and macrophages around the CNV lesions was analyzed with ImageJ64 software (NIH).

2.6. Intravital microscopy of the murine cremaster muscle

For monitoring the leukocyte trafficking on the vascular endothelium in microvessels of the murine cremaster muscle, intravital microscopy was performed. The surgical preparation was performed as described by Baez with minor modifications [29,30]. Mice were injected with vioprolide A (0.1 mg/kg; i.v. *via* the tail vein) or drug vehicle and local inflammation was induced by intrascrotal injection of TNF (500 ng/ml in PBS). DMSO in a concentration of 0.01% (v/v) served as vehicle and was applied to the control group. 6 h post injection, the mice were anesthetized using a ketamine/xylazine mixture (100 mg/kg ketamine, 10 mg/kg xylazine). Subsequently, intravital microscopy of the post-capillary venules of the cremaster muscle was performed with an Olympus BX 50 upright microscope (Olympus Microscopy, Hamburg, Germany). Neutrophils and classical monocytes were identified by *in vivo* immunostaining with an intravenously injected fluorescence-labeled anti-Gr-1 mAb (Biolegend, San Diego, CA, USA). The leukocyte trafficking was analyzed using the AxioVision 4.6 software (Zeiss MicroImaging, Jena, Germany). Off-line analysis of parameters describing the sequential steps of leukocyte extravasation was performed with the AxioVision 4.6 software (Zeiss MicroImaging GmbH). ImageJ software (National Institutes of Health, Bethesda, MD, USA) was used for further image processing and analysis. Rolling leukocytes were defined as those moving slower than the associated blood flow and quantified for 30 s. Firmly adherent cells were determined as those resting in the associated blood flow for $>$ 30 s and related to the luminal surface per 100 μm vessel length. Transmigrated cells were counted in regions of interest, covering 75 μm on both sides of a vessel with $>$ 100 μm length. By measuring the distance between several images of one fluorescent bead (administered *via* the femoral catheter) under stroboscopic illumination, centerline blood flow velocity was determined. From measured vessel diameters and centerline blood flow velocity, apparent wall shear rates were calculated, assuming a parabolic flow velocity profile over the vessel cross-section.

2.7. Cytotoxicity assays

To exclude potential compound-induced (cyto-)toxic effects on HUVECs, a set of cell viability assays was performed.

For analysing the metabolic activity of vioprolide A-treated HUVECs, the CellTiter-Blue cell viability assay (Promega, Mannheim, Germany) was used according to the manufacturer's instructions. In brief, HUVECs were grown to confluence on collagen G (10 μg/ml; Biochrom)-coated 96-well plates (Sarstedt) and treated as indicated. 4 h before the end of the incubation period the CellTiter Blue reagent was added to the cells in a dilution of 1:10. Fluorescence intensity was measured using a microplate reader (SPECTRAFluor Plus; Tecan, Männedorf, Switzerland) at 535 nm (ex) and 590 nm (em).

Cell death was determined by measuring the lactate dehydrogenase (LDH) release from vioprolide A-treated HUVECs using the CytoTox 96 non-radioactive cytotoxicity assay kit (Promega) according to the manufacturer's instructions. Briefly, HUVECs were grown to confluence on collagen G (10 μg/ml; Biochrom) coated 96-well plates (Sarstedt) and treated as indicated. Subsequently, supernatants were incubated with a substrate solution for 30 min. The enzymatic reaction was stopped, and absorbance measurement was performed at 490 nm using a Varioscan Flash microplate reader (Thermo Fisher Scientific, Schwerte, Germany). Cell lysis solution was used as positive control for maximum LDH release into the surrounding medium.

Late apoptosis of vioprolide A-treated HUVECs was investigated by propidium iodide (PI) staining according to Nicoletti et al. [31] Briefly, HUVECs were grown to confluence on collagen G (10 μg/ml; Biochrom)-coated 24-well plates (Sarstedt) and treated as indicated. Subsequently, supernatants were collected and HUVECs were detached using a trypsin/EDTA solution (Biochrom). Cells were washed with ice-cold PBS and incubated with a solution containing 50 μg/ml PI (Sigma-Aldrich), 0.1% Triton X-100 (Sigma-Aldrich) and 0.1% sodium citrate (Carl Roth, Karlsruhe, Germany) for a minimum of 2 h in the dark. Staurosporine (Stsp; Sigma-Aldrich) served as positive control for the induction of apoptosis and was added to non-treated cells in a concentration of 1 μM for 24 h. The percentage of cells with subdiploidic DNA content was analyzed by recording median values for 10.000 events per sample using a FACSVerse flow cytometer (BD Biosciences, San Jose, CA, USA).

2.8. Cell adhesion assay

The adhesion of leukocytes to vioprolide A treated HUVECs was investigated under static conditions. HUVECs were grown to confluence in collagen G (10 μg/ml; Biochrom)-coated 24-well plates (Sarstedt), or in the case of NOP14 knockdown experiments in collagen G (10 μg/ml; Biochrom)-coated 48-well plates (Sarstedt) and treated as indicated. After the treatment period, HUVECs were washed with PBS containing Ca^{2+} and Mg^{2+} to remove all residues of vioprolide A and TNF before 1×10^5, or in the case of NOP14 knockdown experiments 5×10^4, CellTracker Green (Thermo Fisher Scientific)-labeled THP-1 cells, Jurkat cells, PBMCs or PLs were added to the HUVEC monolayer. The leukocytes were allowed to adhere (THP-1, Jurkat: 5 min; PBMCs, PLs: 10 min). Non-adherent leukocytes were washed off using PBS containing Ca^{2+} and Mg^{2+}. The relative amount of adhered fluorescence-labeled THP-1 cells, Jurkat cells, PBMCs and PLs was determined using a microplate reader (SPECTRAFluor Plus; Tecan) at 485 nm (ex) and 535 nm (ex).

2.9. Transmigration assay

1×10^5 HUVECs were grown for 24 h on collagen G (10 μg/ml; Biochrom)-coated Transwell inserts (growth area 0.33 cm^2, 5 μm pore size, polycarbonate; Corning, NY, USA) and treated as indicated. Subsequently, 2×10^4 CellTracker Green (Thermo Fisher Scientific)-labeled THP-1 cells in M199 (PAN-Biotech) supplemented with 0.1% bovine serum albumin (BSA; MilliporeSigma Burlington, MA, USA), 100 U/ml penicillin and 100 μg/ml streptomycin (PAN-Biotech) were added to the upper compartment of the Transwell system. SDF-1 (PeproTech) served as chemoattractant for leukocytes and was added to the lower compartment of the Transwell system to a final concentration of 500 ng/ml in M199 (PAN-Biotech) supplemented with 0.1% BSA (MilliporeSigma), 100 U/ml penicillin and 100 μg/ml streptomycin (PAN-Biotech). THP-1 cells were allowed to migrate through the endothelial monolayer towards the chemoattractant for 2 h. Non-migrated THP-1 cells in the upper compartment were removed using a cotton swap, and transmigrated THP-1 cells were lysed using RIPA buffer and fluorescence intensity was determined using a microplate reader (SPECTRAFLuor Plus, Tecan) at ex 485 nm and em 535 nm.

2.10. Flow cytometry

For investigating the cell surface expression of ICAM-1, VCAM-1, and E-selectin, HUVECs were grown to confluence in collagen G (10 μg/ml; Biochrom)-coated 12-well plates (Sarstedt) and treated as indicated. Subsequently, cells were washed with PBS and detached using HyClone HyQTase (GE Healthcare, Freiburg, Germany). HUVECs were stained for 45 min on ice in the dark for mouse anti-human ICAM-1 (FITC, 1:33, MCA1615F; Bio Rad, Hercules, CA, USA), mouse anti-human VCAM-1 (PE, 1:20, 555647; BD Biosciences) or mouse anti-human E-selectin (PE, 1:10, 551145; BD Biosciences). Protein surface expression was quantified by recording median values for 10.000 events per sample using a FACSVerse flow cytometer (BD Biosciences).

2.11. Quantitative real-time PCR

HUVECs were grown to confluence on collagen G (10 μg/ml; Biochrom)-coated 6-well plates (Sarstedt) and treated as indicated. Subsequently, RNA was isolated using the RNeasy Mini Kit (Qiagen, Hilden, Germany) according to the manufacturer's protocol. On-column DNase digestion was performed with the RNase-Free DNase Set (Qiagen) to remove genomic DNA. 1 μg of the obtained RNA was reverse-transcribed into cDNA using SuperScript II reverse transcriptase (Life Technologies, Darmstadt, Germany). Quantitative real-time PCR was performed according to the comparative C_T quantitation method $2^{-\Delta\Delta Ct}$ using the SYBR Green PCR Master Mix (Life Technologies) and a StepOnePlus System (Applied Biosystems, CA, USA). *GAPDH* served as housekeeping gene. Data were analyzed using the StepOnePlus Software v2.3. The following primer pairs were used: *ICAM1* (forward: 5′- CTG CTC GGG GCT CTG TTC-3′; reverse: 5′-AAC AAC TTG GGC TGG TCA CA-3′), *VCAM1* (forward: 5′-CCA CAG TAA GGC AGG CTG TAA-3′; reverse: 5′-GCT GGA ACA GGT CAT GGT CA-3′), *SELE* (forward: 5′-AGA TGA GGA CTG CGT GGA GA-3‘; reverse: 5′-GTG GCC ACT GCA GGA TGT AT-3′), *TNFRSF1A* (forward: 5′-CAA GCC ACA GAG CCT AGA CA-3′; reverse: 5′-GAA TTC CTT CCA GCG CAA CG-3′), *NFKBIA* (forward: 5′-AGC TCC GAG ACT TTC GAG GA-3′; reverse: 5′-GAG TCA GGA CTC CCA CGC T-3′), *KPNA2* (forward: 5′- GCA GCA ATG TGG AAA ATC AGC-3′; reverse: 5′- TTC GGA ATC AAA CCA GCC CG-3′), *KPNA4* (forward: 5′-CAT TTG GTT CCT CTG CTC AGC C-3′; reverse: 5′-CTT GTG TTT GCT CAT CAG TTC CAG-3′), *KPNB1* (forward: 5′-CTG CTT CCT GAA GCT GCC ATC A-3′; reverse: 5′-CTT CAG CCA GAC TGG AGA AAG C-3′), *GAPDH* (forward: 5′-CCA CAT CGC TCA GAC ACC AT-3′; reverse: 5′-TGA AGG GGT CAT TGA TGG CAA-3′).

2.12. Western blot analysis

HUVECs were grown to confluence on collagen G (10 μg/ml; Biochrom)-coated 6-well plates (Sarstedt) and treated as indicated. Subsequently, cells were washed with cold PBS and lysed with RIPA lysis buffer supplemented with protease and phosphatase inhibitors (4 mM Complete Mini EDTA-free (Roche, Mannheim, Germany), 0.3 mM sodium orthovanadate (Sigma-Aldrich), 1 mM sodium fluoride (Merck Millipore, Darmstadt, Germany), 1 mM PMSF (Roche Diagnostics, IN, USA), 3 mM β-glycerophosphate (Sigma-Aldrich), 10 mM sodium pyrophosphate (Sigma-Aldrich), 0.12% (v/v) H_2O_2 (Sigma-Aldrich)). The protein content of each individual sample was detected using the Pierce BCA Protein Assay Kit (Thermo Fisher Scientific) and a pyronin-based sample buffer containing sodium dodecyl sulphate (SDS) was added to the samples followed by incubation at 95 °C for 5 min. Equal amounts of protein (20–40 μg) were separated by sodium dodecyl sulphate-polyacrylamide gel electrophoresis (SDS-PAGE; Bio-Rad Laboratories, Munich, Germany) and transferred onto a polyvinylidene fluoride membrane (PVDF; Bio-Rad) by semi-dry electroblotting using the Trans-Blot Turbo Transfer System (Bio-Rad) at constant voltage (25 V) for 30 min. Unspecific binding sites were blocked with 5% non-fat dry milk (Blotto; Carl Roth) or 5% BSA (MilliporeSigma) containing 0.1% Tween-20 (Sigma-Aldrich), respectively. The following primary antibodies were used: rabbit anti-human ICAM-1 (1:2000, #4915; Cell Signaling/New England Biolabs, Frankfurt am Main, Germany), mouse anti-human VCAM-1 (1:1000, sc13160; Santa Cruz Biotechnology, Dallas, TX, USA), mouse anti-human E-selectin (1:1000, sc137054; Santa Cruz Biotechnology), rabbit anti-human TNFR1 (1:750, #3736; Cell Signaling/New England Biolabs), rabbit anti-human phospho-TAK1 (Thr184/187) (1:250, #4508; Cell Signaling/New England Biolabs), rabbit anti-human TAK1 (1:250, #4505; Cell Signaling/New England Biolabs), rabbit anti-human phospho-IKKα/β (1:500, #2697; Cell Signaling/New England Biolabs), rabbit anti-human IKKβ (1:500, #8943; Cell Signaling/New England Biolabs), rabbit anti-human phospho-IκBα (Ser32) (1:1000, #2859; Cell Signaling/New England Biolabs), rabbit anti-human IκBα (1:2000, #9242; Cell Signaling/New England Biolabs), mouse anti-human NF-κB p65 (1:1000, sc8008; Santa Cruz Biotechnology), rabbit anti-human importin subunit alpha-1 (1:1000, #14372; Cell Signaling/New England Biolabs), mouse anti-human importin subunit alpha-3 (1:1000, sc390535; Santa Cruz Biotechnology), rabbit anti-human importin beta-1 (1:1000, #60769; Cell Signaling/New England Biolabs) and rabbit anti-human NOP14 (1:2000, PA5–58851; Invitrogen, Thermo Fisher Scientific). For unconjugated primary antibodies, the secondary antibodies goat anti-rabbit linked to HRP (1:3000, #7074; Cell Signaling/New England Biolabs) and goat anti-mouse linked to HRP (1:3000, #7076, Cell Signaling/New England Biolabs) were used. For loading control, rabbit anti-human β-tubulin (1:1000, #2128; Cell Signaling/New England Biolabs), mouse anti-human topoisomerase 1 (1:1000, sc271285; Santa Cruz Biotechnology) or mouse anti-human β-actin-peroxidase (1:100.000, A3854; Sigma Aldrich) was used. Protein expression was detected by chemiluminescence measurement and quantification of protein expression was performed by densitometric analysis of protein bands using ImageJ (software version 1.49k).

2.13. De novo protein synthesis assay

HUVECs were grown to confluence on collagen G (10 μg/ml; Biochrom) coated 8-well μ-slides (ibidi, Martinsried, Germany) and treated as indicated. CHX (Sigma-Aldrich) served as positive control for the inhibition of mRNA translation. To analyze *de novo* protein synthesis, the Click-iT Plus OPP Alexa Fluor 488 Protein Synthesis Assay Kit (Thermo Fisher Scientific) was used according to the manufacturer's instructions. In brief, 20 μM Click-iT O-propargyl-puromycin (OPP) was added to the cells for the last 30 min of treatment leading to the incorporation of OPP into newly synthesized proteins. Subsequently, cells were fixed with 4% formaldehyde (Roti-Histofix; Carl Roth) and permeabilized with 0.5% Triton X-100 for 15 min. The incorporated OPP was labeled with Alexa Fluor 488 to visualize the newly synthesized proteins. Microscopical images were obtained using a Leica DMI6000B fluorescence microscope (Leica Microsystems, Wetzlar, Germany). The intensity of the Click-iT OPP signal in the nucleus was normalized to the intensity of the cell nuclei staining (NuclearMark Blue Stain) and analyzed using ImageJ (software version 1.49k).

2.14. Cell fractionation

For analyzing the cellular distribution of proteins, cells were separated into a cytosolic and nuclear fraction. In brief, HUVECs were grown to confluence on collagen G (10 μg/ml; Biochrom) coated 10 cm dishes (Sarstedt) and treated as indicated. Subsequently, cells were washed with ice-cold PBS, scraped off the dish and centrifuged at 17.000 g for 1 min. The cell pellet was resuspended in fractionation buffer A consisting of 10 mM Hepes pH 7.9 (Carl Roth), 10 mM potassium chloride (Merck Millipore), 0.1 mM EDTA (Sigma-Aldrich), 0.1 mM EGTA (Sigma-Aldrich), 4 mM Complete Mini EDTA-free (Roche), 1 mM PMSF (Roche) and 1 mM DTT (Sigma-Aldrich) and incubated for 15 min on ice. Nonidet P-40 (Sigma-Aldrich) was added to each sample to a final concentration of 0.75% (v/v). The samples were briefly vortexed followed by

centrifugation at 17.000 g for 1 min. The supernatant, containing cytosolic proteins, was transferred to a new tube. The remaining cell pellet was incubated with fractionation buffer C consisting of 20 mM Hepes pH 7.9 (Carl Roth), 0.4 M sodium chloride (Carl Roth), 1 mM EDTA (Sigma-Aldrich), 1 mM EGTA (Sigma-Aldrich), 1% Nonidet P-40 (Sigma-Aldrich), 4 mM Complete Mini EDTA-free (Roche), 1 mM PMSF (Roche) and 1 mM DTT (Sigma-Aldrich) and incubated for 15 min on ice. Samples were centrifuged at 17.000 g for 5 min, and the supernatant, which contained nuclear proteins, was transferred to a fresh tube. The protein content of each sample was determined using the Pierce BCA Protein Assay Kit (Thermo Fisher Scientific) according to the manufacturer's instructions. A pyronin-based sample buffer containing SDS was added to the samples followed by incubation at 95 °C for 10 min. Equal amounts of protein (40–50 μg) were used for Western blot analysis as described in Section 2.12. Topoisomerase I and β-tubulin served as markers for the purity of the nuclear and cytosolic fraction, respectively.

2.15. Immunofluorescence staining

HUVECs were grown to confluence on collagen G (10 μg/ml; Biochrom)-coated 8-well μ-slides (ibidi) and treated as indicated. Subsequently, the cells were fixed with 4% formaldehyde (Roti-Histofix; Carl Roth) and permeabilized with 0.2% Triton X-100 for 2 min (NF-κB p65) or 5 min (importin subunit alpha-1). Unspecific binding sites were blocked with 0.2% BSA (MilliporeSigma) for 30 min and cells were treated with primary antibody for 2 h. The following primary antibodies were used: rabbit anti-human NF-κB p65 (1:400, sc8008; Santa Cruz Biotechnology) and rabbit anti-human importin subunit alpha-1 (1:400, #14372; Cell Signaling/New England Biolabs). The cells were washed with PBS to remove unbound primary antibody followed by incubation with an Alexa Fluor 488 conjugated secondary antibody (goat anti-mouse, 1:400, A11001 or goat anti-rabbit, 1:400, A11008; Thermo Fisher Scientific) for 2 h in the dark. Immunofluorescence staining was detected using a Leica DMI6000B fluorescence microscope (Leice Microsystems) and image quantification was performed using ImageJ (software version 1.49k) allowing determination of NF-κB p65 and importin subunit alpha-1 nuclear translocation.

2.16. NF-κB promotor activity

To analyze the NF-κB promotor activity, 1×10^6 HUVECs were transfected in aluminum cuvettes with the *Firefly* luciferase reporter plasmid pGL4.32[luc2P/NF-κB-RE/Hygro] (Promega) and a *Renilla* control plasmid pGL4.74[hRluc/TK] (Promega) at a ratio of 10:4 by electroporation using the Amaxa Nucleofector 2b device and the Human Umbilical Vein Endothelial Cell Nucleofector Kit (Lonza, Basel, Switzerland). The transfected cells were seeded into collagen G (10 μg/ml; Biochrom)-coated 48-well plates (Sarstedt). After 24 h, the transfected HUVECs were treated as indicated followed by lysis of the cells with passive lysis buffer. The NF-κB promotor activity was measured using the Dual-Luciferase Reporter Assay System (Promega) according to the manufacturer's protocol using a luminometer (SPECTRAFluor Plus, Tecan).

2.17. Cellular thermal shift assay (CETSA)

The cellular thermal shift assay was performed as described previously [32] with the following modifications: Confluent HUVECs were treated with 300 nM vioprolide A for 1 h or left untreated. Cells were detached using trypsin/EDTA solution (Biochrom), washed with ice-cold PBS, and the cell number was adjusted to 5.8×10^6 cells per milliliter. 5.8×10^5 cells each were heated with eight temperature endpoints between 42.3 °C and 57.8 °C for 3 min using a peqSTAR thermocycler (PEQLAB Biotechnology, Erlangen, Germany). Cells were incubated at 21 °C for another 3 min and snap-frozen in liquid nitrogen immediately after. Cell lysis was performed by repeated freeze-thaw cycles in liquid nitrogen and the insoluble fraction containing denatured proteins was separated by centrifugation at 20.000 g for 30 min 3x SDS Sample Loading Buffer (187.5 mM Tris-HCl (pH 6.8), 6% (w/v) SDS, 30% glycerol, 150 mM DTT, 0.03% (w/v) bromophenol blue, 2% β-mercaptoethanol) was added to the supernatants followed by incubation at 95 °C for 5 min. Thermal aggregation curves of NOP14 were determined by western blot analysis as described in Section 2.12.

2.18. siRNA transfection

For investigating the influence of NOP14 knockdown on activated endothelial cells, HUVECs were transfected with ON-TARGET plus human NOP14 siRNA smart pool (Dharmacon/Horizon Discovery, Lafayette, CO, USA) or siGENOME control pool (Dharmacon/Horizon Discovery) as transfection control using the GeneTrans II Transfection Reagent (MoBiTec, Goettingen, Germany) and the DNA Diluent B (MoBiTec) according to the manufacturer's instructions. Briefly, HUVECs were seeded in a concentration of 25.000 cells/cm^2 growth area and allowed to grow for 24 h in ECGM supplemented with 10% FCS (Biochrom), 100 U/ml penicillin, 100 μg/ml streptomycin (PAN-Biotech), 2.5 μg/ml amphotericin B (PAN-Biotech) and supplement mixture (PELOBiotech). For cell adhesion assays, 48-well plates (Sarstedt) and for immunofluorescence staining 8-well μ-slides (ibidi) were used. After 24 h, the medium was changed to ECGM containing 100 U/ml penicillin, 100 μg/ml streptomycin (PAN-Biotech) and 10 mM L-glutamine (Thermo Fisher Scientific). A final concentration of 60 nM siRNA in combination with the GeneTrans II Transfection Reagent and DNA Diluent B was added to the cells. 4 h post transfection, the medium was changed back to ECGM containing 10% FCS (Biochrom), 100 U/ml penicillin, 100 μg/ml streptomycin (PAN-Biotech), 2.5 μg/ml amphotericin B (PAN-Biotech) and supplement mixture (PELOBiotech), and 24 h post transfection the medium was exchanged once more.

2.19. Statistical analysis

The number of independently performed experiments (n) indicates different donors for primary cells. All experiments were performed independently for at least three times; the actual number of performed experiments is stated in the respective figure legends. Statistical analyses were performed using GraphPad Prism software version 5.0 (San Diego, USA). One-way ANOVA followed by Tukey's *post hoc* test or unpaired Student's *t*-test was used for the evaluation of significant differences. $P \leq 0.05$ was considered as statistically significant. Data are expressed as mean ± standard error of the mean (SEM).

3. Results

3.1. Vioprolide A attenuates inflammatory actions in murine models in vivo

For studying the anti-inflammatory actions of vioA *in vivo*, two distinct murine inflammatory models were used. First, we investigated the infiltration of microglia and macrophages, which take part in the inflammatory response during laser-induced choroidal neovascularization. Immunostaining of RPE/choroid flat mounts from laser-induced choroidal neovascularization (CNV)-treated eyes with allograft inflammatory factor 1 (AIF1 or Iba1), which is upregulated in activated microglia and macrophages [33], revealed that vioA treatment (30 nM) lead to a significant reduction (approx. 50%) in the number of Iba1-positive laser lesion area-infiltrating microglia and macrophages compared to control treatment (Figs. 1a and S1). In the next step, we focused on the interaction of leukocytes with vascular endothelial cells, which is needed for the extravasation of the leukocytes into the inflamed tissue. The rolling, adhesion and transmigration of Gr-1^+ neutrophils and classical monocytes was investigated by intravital microscopy of the

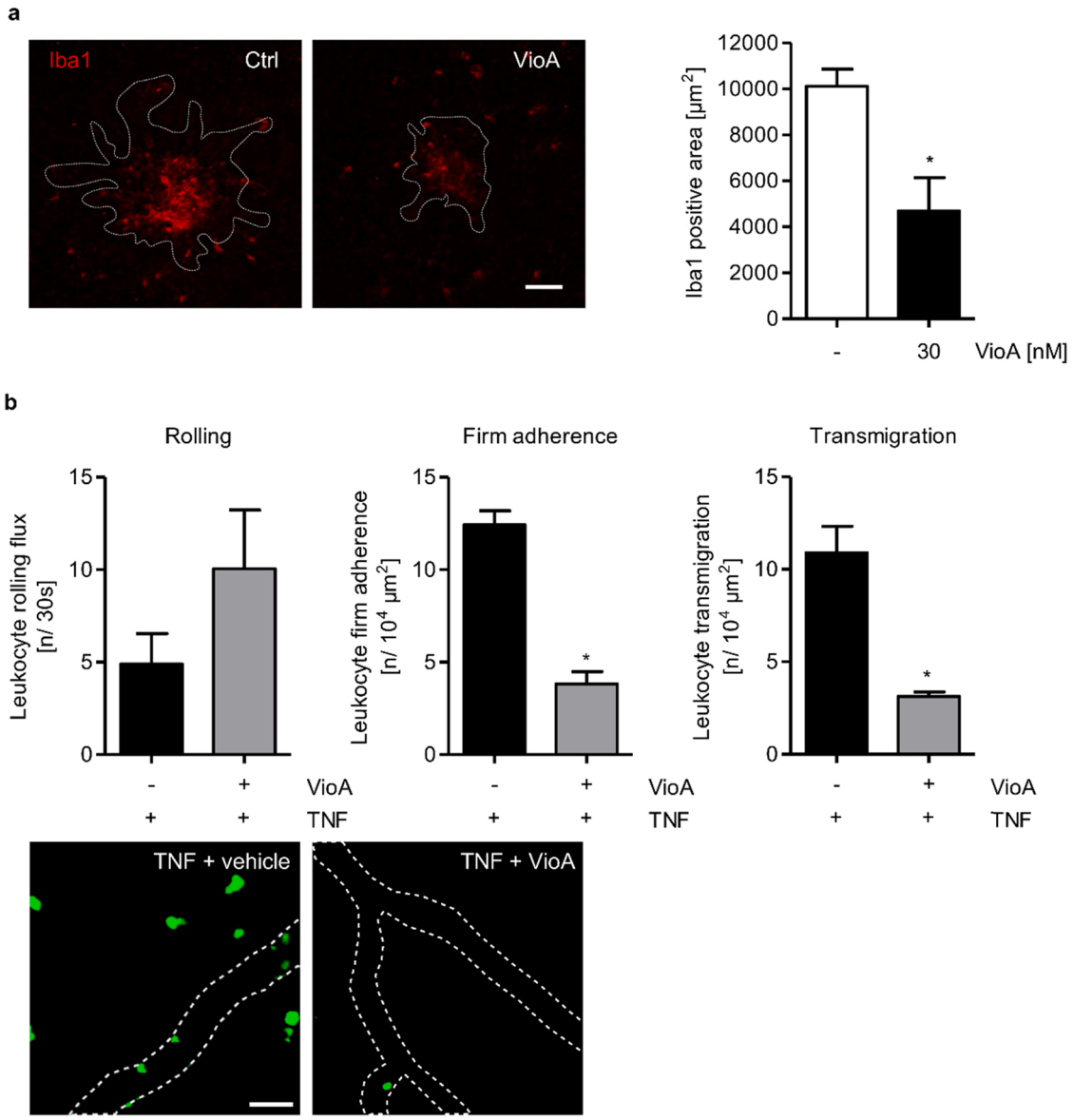

Fig. 1. Vioprolide A reduces the microglia and macrophage infiltration in a laser-induced choroidal neovascularization model and the adhesion and transmigration of leukocytes in the cremaster muscle in mice *in vivo*. a Laser-induced choroidal neovascularization model. Mice were intravitreally injected with vioprolide A (30 nM) or vehicle (0.03% DMSO in 0.9% NaCl). Laser photocoagulation was conducted immediately after injection and the infiltration of microglia and macrophages around the CNV lesions was determined on day 14 by visualizing Iba1 using immunohistochemistry and fluorescence microscopy. CNV lesions are shown in dotted lines. One representative experiment out of 3 is shown. Scale bar, 50 µm. b Intravital microscopy of the cremaster muscle in mice. Mice were injected with vioprolide A (0.1 mg/kg, i.a.) or vehicle (0.02% DMSO). After 1 h, TNF (300 ng) was applied intrascrotally. After 4 h, the TNF-evoked rolling, firm adhesion and transmigration of Gr-1$^+$ neutrophils and classical monocytes to the postcapillary venules of the cremaster muscle were detected by intravital microscopy. One representative intravital microscopic image is shown. Vessel walls are depicted as dotted lines. Scale bar, 100 µm. IBA1, ionized calcium-binding adapter molecule 1; VioA, vioprolide A. Data are expressed as mean ± SEM. n = 6 (a) and n = 8 (b). *$P \leq 0.05$ *vs.* negative control (a) or TNF control (b).

TNF-activated cremaster muscle in mice. An example of the quantification method is given in Suppl. Fig. S2. VioA treatment (0.1 mg/kg) caused a significant decrease (approx. 70%) of the leukocyte adhesion to and transmigration through the vascular endothelium (Fig. 1b). The leukocyte rolling, however, was not affected. Taken together, these data demonstrate that vioA elicits potent anti-inflammatory actions *in vivo*.

3.2. Vioprolide A lowers leukocyte-endothelial cell interactions in vitro

For more profound investigations concerning the anti-inflammatory properties of vioA on endothelial cells *in vitro*, we first performed cell viability assays to ensure that the effects of vioA are not linked to (cyto-) toxicity. We found that concentrations up to 10 nM of vioA for a maximum of 72 h had no effect on the metabolic activity Fig. S3a), membrane integrity Fig. S3b) and apoptosis rate (Fig. S3c) of HUVECs. In the next step, the leukocyte-endothelial cell interaction was examined *in vitro* by focusing on the leukocyte adhesion to and transmigration through a TNF-activated monolayer of HUVECs. Note that only endothelial cells were treated with vioA, whereas the leukocytes remained untreated to focus solely on the anti-inflammatory actions of vioA in endothelial cells. As shown in Fig. 2a, the adhesion of fluorescently labeled THP-1 cells, Jurkat cells, PLs and PBMCs to a TNF-activated HUVEC monolayer was significantly downregulated when HUVECs were pretreated with vioA for 16 h. The reduction of leukocyte adhesion

was concentration-dependent with the highest effect observed for 10 nM of vioA. In addition, the leukocyte transmigration through a TNF-activated endothelial monolayer towards an SDF-1 gradient was significantly decreased after pretreatment of the HUVECs with 10 nM vioA for 16 h (Fig. 2b). Taken together, we showed that the treatment of endothelial cells with vioA caused a significant reduction of leukocyte-endothelial cell interactions *in vitro*.

3.3. Vioprolide A reduces the expression levels of endothelial cell adhesion molecules in vitro

CAMs play a crucial role in mediating leukocyte-endothelial cell interaction. While E-selectin is involved in the rolling motion of leukocytes on the endothelial surface, ICAM-1 and VCAM-1 mediate the firm adhesion of the leukocytes to the endothelium. As we could show a reduction of the leukocyte adhesion to and transmigration through a TNF-activated endothelial monolayer, we next focused on the effects of vioA on the expression level of the endothelial CAMs to uncover the underlying mode of action of the anti-inflammatory actions of vioA.

Via flow cytometry we monitored the cell surface protein levels of ICAM-1, VCAM-1 and E-selectin on TNF-activated HUVECs. These levels were significantly downregulated after vioA pretreatment (16 h; Fig. 3a). The observed reduction was concentration-dependent and almost completely inhibited at the highest vioA concentration applied (10 nM). To further differentiate if vioA impairs the trafficking of CAMs to the cell surface or rather the overall protein expression of CAMs, the total protein level of ICAM-1, VCAM-1 and E-selectin in TNF-activated HUVECs was analyzed by western blot experiments (Fig. 3b). In accordance with the results obtained for the cell surface expression, the total protein levels of all three CAMs were significantly reduced when HUVECs were pretreated with vioA for 16 h. Again, the observed effects were concentration-dependent and the highest concentration of vioA (10 nM) completely inhibited the TNF-induced total protein expression of ICAM-1, VCAM-1 and E-selectin. In addition to influencing the total protein expression of CAMs, we found that pretreatment with vioA (16 h) also decreased the TNF-induced mRNA expression of *ICAM1* and *VCAM1* after 4 h and of *SELE* after 2 h in HUVECs (Fig. 3c). However, in contrast to the effect on the protein level of CAMs, the highest applied concentration of vioA (10 nM) was not able to completely downregulate the TNF-induced mRNA expression. Similar effects on the mRNA expression of CAMs in HUVECs was also observed after 16 h of vioA pretreatment followed by 4 h (*SELE*) and 6 h (*ICAM1*, *VCAM1*) of TNF activation (Suppl. Fig. S4). In total, we could demonstrate that the action of vioA observed on the leukocyte-endothelial cell interaction is likely to be caused through impairment of CAMs in HUVECs. The reduced protein expression of CAMs, however, can only in part be attributed to a reduced TNF-induced mRNA expression.

3.4. Vioprolide A impairs de novo protein synthesis in HUVECs leading to reduced TNFR1 protein levels

Due to the observed discrepancy between the protein and mRNA expression of CAMs and based on recently published data showing that vioA interacts with NOP14, which is involved in the ribosomal biogenesis and assembly of the small subunit processome, we examined the effect of vioA on general *de novo* protein synthesis in HUVECs using a protein translation assay. As shown in Fig. 4a and b, the formation of newly synthesized proteins in HUVECs was both concentration- and time-dependently impaired upon vioA treatment. A maximum inhibitory effect was observed after treatment for 16 h with 10 nM, which was equally strong compared to the treatment with the known protein synthesis inhibitor cycloheximide (CHX, 10 μg/ml) for 24 h. Concentration-response curves of vioA (Suppl. Fig. S5a) and CHX (Suppl. Fig. S5b) further indicated that 10 nM of vioA and 3 μg/ml of CHX applied over a

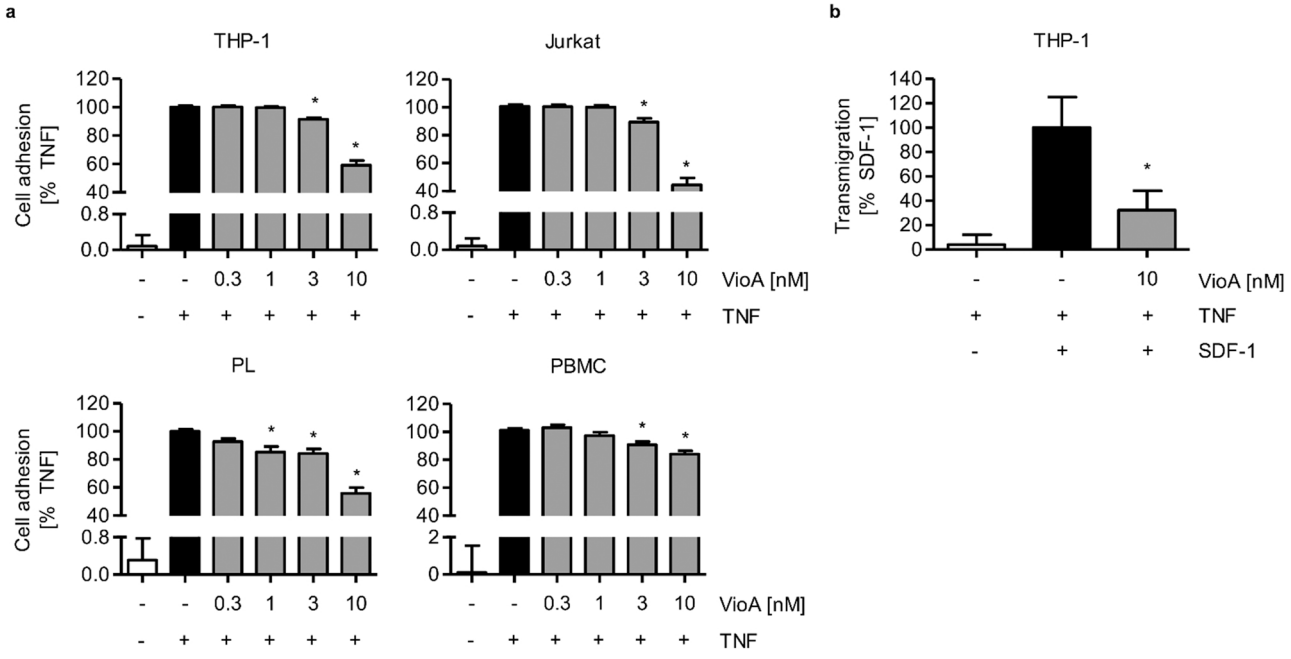

Fig. 2. Vioprolide A reduces the leukocyte adhesion to and transmigration through a HUVEC monolayer *in vitro*. a Confluent HUVECs were treated with vioprolide A as indicated for 16 h and activated with TNF (10 ng/ml) for 6 h. Fluorescence-labeled THP-1 cells, Jurkat cells, primary lymphocytes (PLs) and peripheral blood mononuclear cells (PBMCs) were allowed to adhere for 5 min (THP-1 cells, Jurkat cells) or 10 min (PLs, PBMCs). The amount of adhered THP-1 cells, Jurkat cells, PLs and PBMCs was analyzed using fluorescence measurement. b HUVECs were grown on the porous membrane of a Transwell insert (pore size 5 μm) for 24 h, treated with vioprolide A as indicated for 16 h and activated with TNF (10 ng/ml) for 6 h. SDF-1 (CXCL12, 500 ng/ml) was added to the lower compartment of the Transwell as chemoattractant. Fluorescence-labeled THP-1 cells were added to the upper compartment of the Transwell and allowed to transmigrate through the HUVEC monolayer for 2 h. The amount of transmigrated THP-1 cells was determined by fluorescence measurement. VioA, vioprolide A. Data are expressed as mean ± SEM. n = 3 (b), n = 5 (a THP-1, a PL, a PBMC), n = 6 (a Jurkat). *P ≤ 0.05 *vs.* TNF control (a) or SDF-1 control (b).

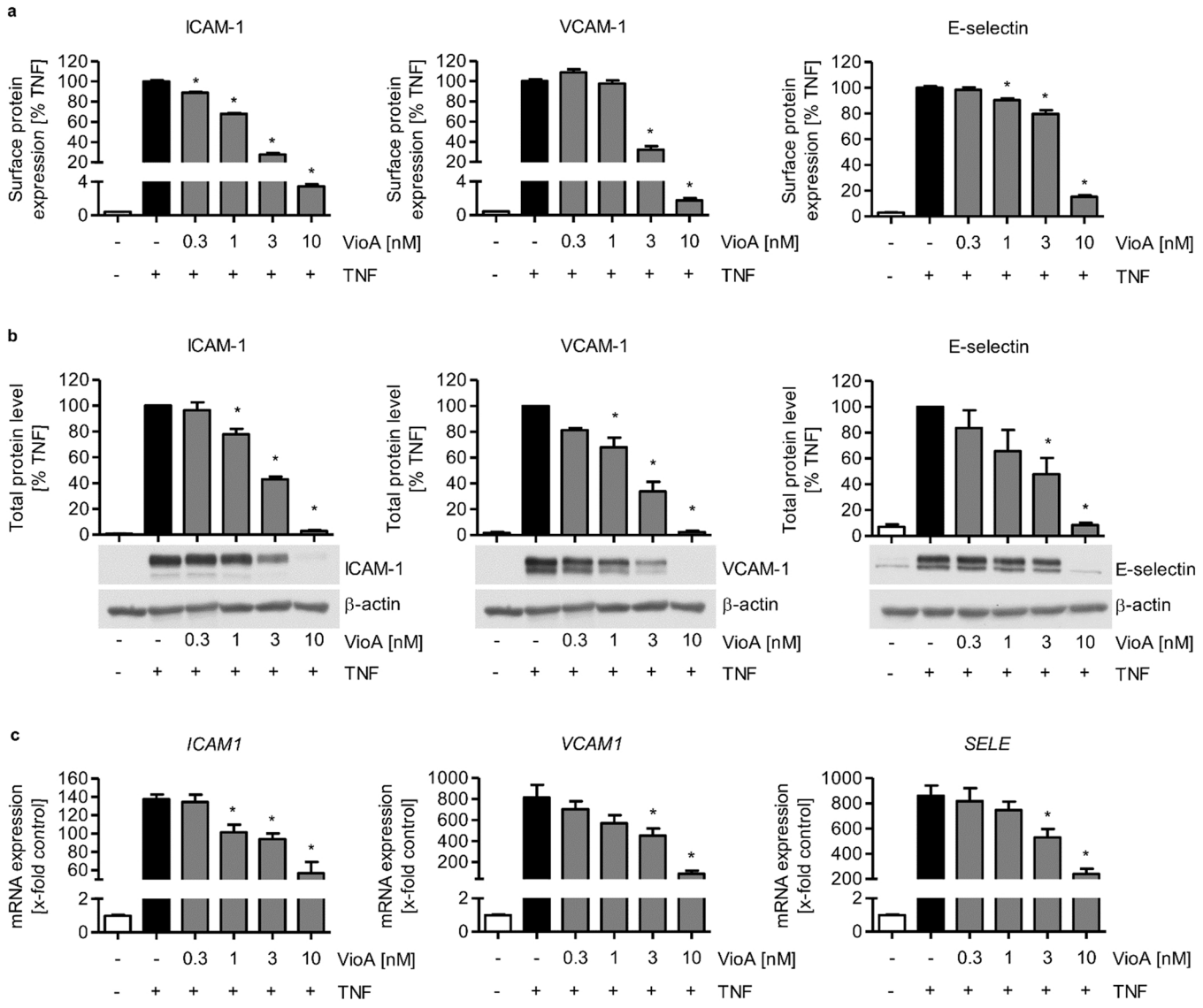

Fig. 3. Vioprolide A reduces ICAM-1, VCAM-1 and E-selectin expression in HUVECs. a-b Confluent HUVECs were treated with the indicated concentrations of vioprolide A for 16 h followed by activation with TNF (10 ng/ml) for 4 h (E-selectin) or 6 h (ICAM-1, VCAM-1). a ICAM-1, VCAM-1 and E-selectin cell surface protein expression was measured by flow cytometry. b Total protein expression of ICAM-1, VCAM-1 and E-selectin was detected by western blot analysis. One representative blot out of 3 is shown. c Confluent HUVECs were treated with vioprolide A as indicated for 16 h followed by activation with TNF (10 ng/ml) for 2 h (*SELE*) or 4 h (*ICAM1*, *VCAM1*). The mRNA expression of *ICAM1*, *VCAM1* and *SELE* was analyzed by quantitative PCR. VioA, vioprolide A. Data are expressed as means ± SEM. n = 3. *P ≤ 0.05 *vs.* TNF control.

period of 16 h had equally potent effects on the *de novo* protein synthesis in HUVECs. It is known that various natural inhibitors of mRNA translation, including the plant alkaloid narciclasine and the bacteria-derived cytotrienin A, exert their anti-inflammatory actions through influencing the TNFR1 [34,35]. The TNFR1 is the most important receptor in TNF-mediated inflammatory signaling in endothelial cells and its activation causes the induction of the downstream NF-κB signaling cascade. For assessing if the anti-inflammatory properties of vioA would derive from impairing the TNFR1, too, we analyzed its protein level in HUVECs upon vioA treatment over a period of 48 h. As demonstrated in Fig. 4c, vioA strongly reduced the TNFR1 protein level in a time-dependent manner. The maximum effect was observed after 16 h of treatment with 10 nM of vioA. This result is in line with the effect on general *de novo* protein synthesis. At the same time, vioA time-dependently upregulated the *TNFRSF1A* mRNA expression in HUVECs (Fig. 4d), underlining that the effect of vioA on the TNFR1 protein level is attributed to an influence on mRNA translation rather than mRNA expression. More detailed investigations regarding the turnover of the TNFR1 were performed by using CHX and revealed a short half-life of the protein of approximately 30 min (Suppl. Fig. S6a left). CHX treatment of up to 72 h completely inhibited the TNFR1 protein expression (Suppl. Fig. S6a right), whereas the TNFR1 protein level recovered after vioA treatment for 24 h or longer. Importantly, when vioA (10 nM) was administered repetitively each 12 h for a total period of 48 h, HUVECs showed no recovery from the protein synthesis inhibition (Suppl. Fig. S6b). In line with this, the TNFR1 protein level did not recover after repetitive treatment with vioA (Suppl. Fig. S6c). These observations indicate that the TNFR1 has on the one hand a short half-life and is on the other hand quickly resynthesized when protein synthesis inhibition is relieved.

3.5. *Vioprolide A inhibits important kinases of the NF-κB signaling pathway but does not rescue IκBα protein levels*

To further asses the role of the reduced TNFR1 protein level in the anti-inflammatory actions of vioA, we investigated the downstream NF-κB signaling pathway. When the TNFR1 is activated, consecutive

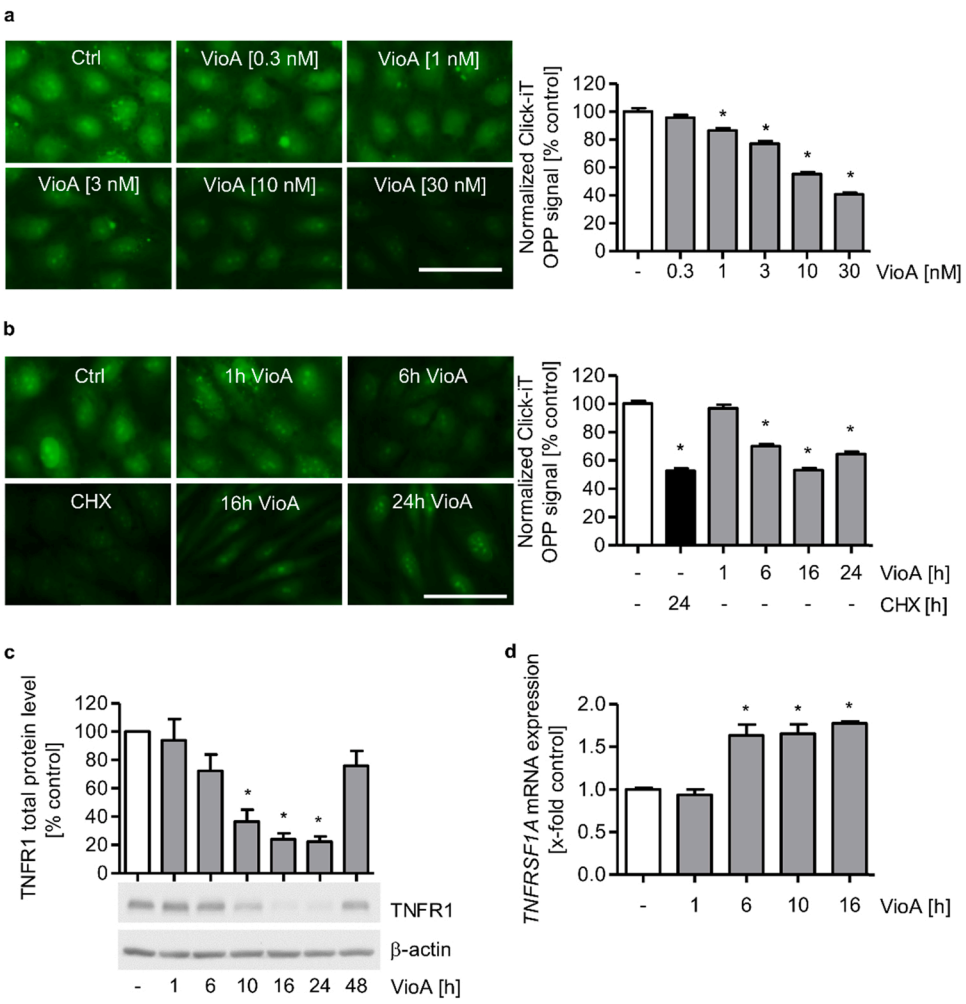

Fig. 4. Vioprolide A impairs *de novo* protein synthesis in HUVECs and downregulates TNFR1 protein expression. a Confluent HUVECs were treated with the indicated concentrations of vioprolide A. b Confluent HUVECs were treated with vioprolide A (10 nM) for the indicated time points. CHX (10 μg/ml) served as positive control. a-b Nascent polypeptide chains were visualized by immunocytochemistry using Click-iT Plus OPP Alexa Fluor 488 and fluorescence microscopy. One representative experiment out of 3 is shown. Scale bar, 50 μm. c-d Confluent HUVECs were treated with vioprolide A (10 nM) for the indicated time points. Total protein expression of TNFR1 (c) was determined by western blot analysis. One representative blot out of 3 is shown. Total mRNA expression of *TNFRSF1A* (d) was detected by quantitative PCR. VioA, vioprolide A; CHX, cycloheximide. Data are expressed as means ± SEM. n = 3. *P ≤ 0.05 *vs.* negative control.

downstream kinases, such as TAK and IKK are induced, which cause IκBα phosphorylation and degradation. In the following, the liberated NF-κB subunits can translocate to the nucleus where they bind to promotor regions and regulate the gene transcription of important inflammatory genes, such as the aforementioned CAMs. As demonstrated in Fig. 5a and 5b, we found that the phosphorylation of TAK and IKK was significantly downregulated in vioA-pretreated (16 h) HUVECs after 15 min, 30 min and 60 min of TNF treatment. Nevertheless, investigations regarding IκBα revealed that pretreatment with vioA (16 h) enhanced the reduction of the IκBα protein levels that was triggered by TNF treatment for 15 min, 30 min and 60 min (Fig. 5c). In addition, the relative amount of IκBα phosphoprotein in TNF-activated HUVECs was decreased upon vioA pretreatment for 16 h (Suppl. Fig. S7a). Based on these findings, we were interested in how vioA alone (without TNF treatment) would impair IκBα total protein levels in HUVECs. As shown in Fig. 5d, the total protein level of IκBα was time-dependently reduced upon vioA treatment. Compared to the rapid decrease of the TNFR1 protein level (Fig. 4c), however, the IκBα protein level decreased more slowly and showed no recovery up to 48 h of vioA treatment. In concert with the results for TNFR1, *NFKBIA* mRNA expression was time-dependently upregulated by vioA (Fig. 5e), which underlines that the effects observed are caused by the influence of vioA on protein synthesis. CHX treatment showed a similar time-dependent influence on the IκBα protein level in HUVECs (Fig. 5f). Importantly, up to 6 h of CHX treatment only evoked a reduction of the IκBα total protein level of about 40% (Suppl. Fig. S7b). This confirms that the protein has a longer half-life compared to the TNFR1. Similar to the results obtained for the TNFR1, repetitive treatment with vioA every 12 h for a total of 48 h decreased the IκBα protein level more than the single treatment for 48 h (Suppl. Fig. S7c). Interestingly, previous data concerning the protein synthesis inhibitor narciclasine demonstrated no effect on the total protein level of IκBα in HUVECs [34]. Taken together, we could show that although vioA reduces the TNFR1 protein level and decreases the TNF-evoked activation of important kinases of the NF-κB signaling cascade, such as TAK and IKK, the natural product does not rescue IκBα protein levels. In contrast, vioA is likely to reduce the IκBα protein levels without TNF-activation due to its inhibitory effect on general *de novo* protein synthesis.

3.6. *Vioprolide A prevents NF-κB p65 nuclear translocation and NF-κB promotor activity*

Because the inhibitory protein IκBα is important for masking the NLS of NF-κB subunits and due to the fact that vioA reduced the IκBα protein level in HUVECs, we next focused on the NF-κB subunit p65. We neither observed an effect on the p65 total protein level over a period of 48 h of vioA treatment, indicating a long half-life of this protein, nor on its cellular distribution in HUVECs, as shown by cellular fractionation and western blot experiments (Fig. 6a). The purity of the subcellular fractions was ensured in each individually performed experiment using western blot analysis of β-tubulin and topoisomerase I as cytosolic and nuclear marker, respectively (Fig. S8a). Surprisingly, despite reduced IκBα protein levels, immunofluorescence staining for the NF-κB subunit p65 revealed that its nuclear translocation in HUVECs was markedly decreased upon vioA pretreatment (16 h) after 15 min, 30 min and 60 min of TNF activation (Fig. 6b). In accordance with this, we could

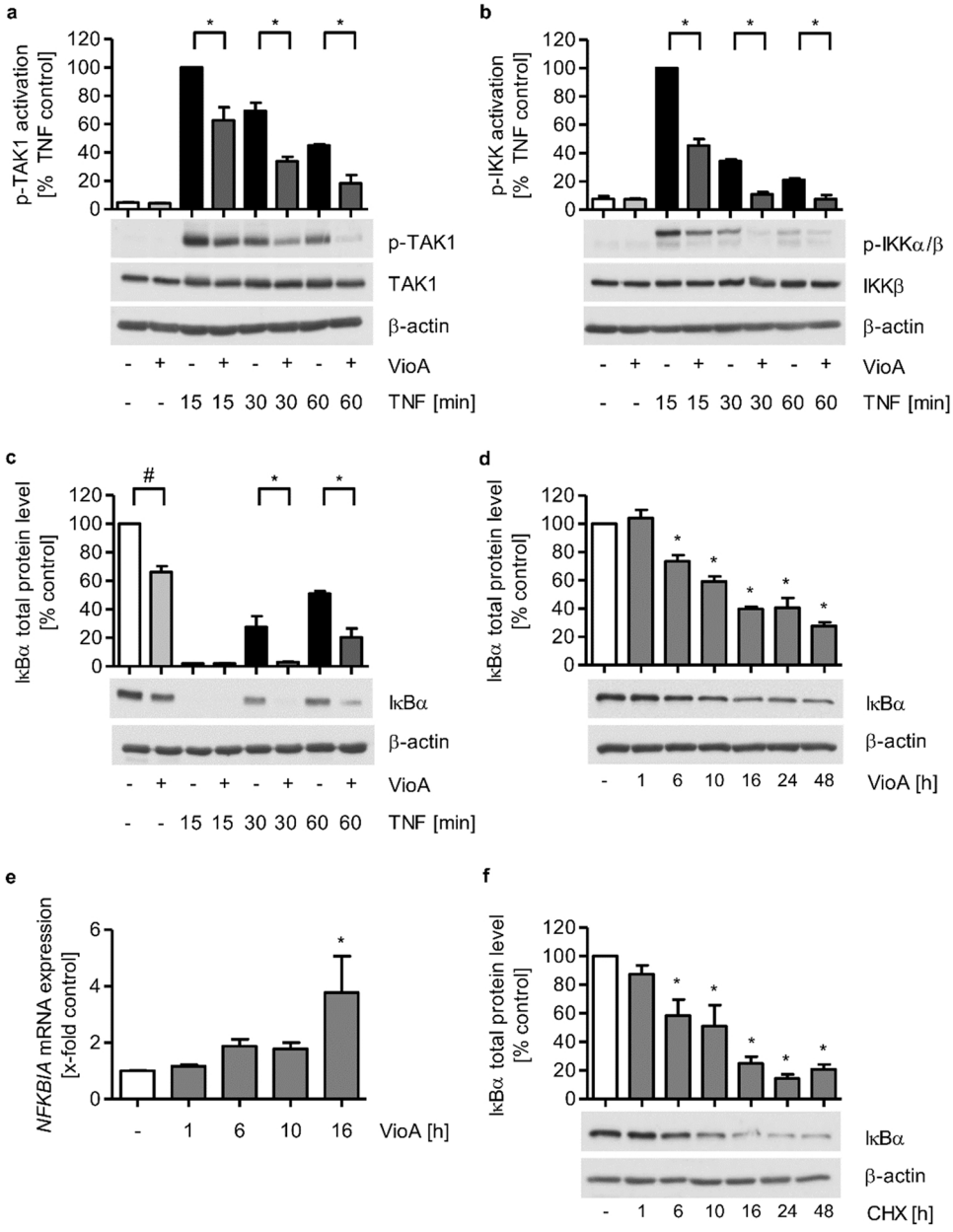

Fig. 5. Vioprolide A reduces the activation of TNFR1 downstream kinases, yet IκBα total protein levels are decreased. a-c Confluent HUVECs were treated with vioprolide A (10 nM) for 16 h followed by activation with TNF (10 ng/ml) for the indicated time points. Total protein expression of phospho-TAK1 (p-TAK1, a), phospho-IKKα/β (p-IKKα/β, b) and IκBα (c) was analyzed by western blot experiments. One representative blot out of 3 is shown. d-e Confluent HUVECs were treated with vioprolide A (10 nM) as indicated. Total protein expression of IκBα (d) was detected by western blot analysis. One representative blot out of 3 is shown. Total mRNA expression of *NFKBIA* (e) was detected by quantitative PCR. f Confluent HUVECs were treated with cycloheximide (3 μg/ml) as indicated. Total protein expression of IκBα was detected by western blot analysis. One representative blot out of 3 is shown. VioA, vioprolide A, CHX, cycloheximide. Data are expressed as means ± SEM. n = 3. *P ≤ 0.05 *vs.* TNF control (a-c) or negative control (d, e, f), #P ≤ 0.05 *vs.* negative control (c).

demonstrate that the TNF-induced NF-κB promotor activity, assessed by NF-κB reporter gene assay, was concentration-dependently reduced upon pretreatment of HUVECs with vioA for 16 h (Fig. 6c). Importantly, although vioA has been assessed as inhibitor of protein synthesis, the expression of the *Renilla* control plasmid remained unaffected, which strengthens the results of the NF-κB reporter gene assay (Fig. S9). In summary, these results indicate that the anti-inflammatory actions of vioA can be attributed to an inhibition of the NF-κB p65 nuclear translocation.

3.7. The inhibition of NF-κB p65 nuclear translocation by vioprolide A is attributed to an impairment of importin family members

Important for the successful nuclear translocation of NF-κB subunits is on the one hand the release of their NLS through degradation of IκBα and on the other hand the interaction with carrier proteins that ensure the shuttling of the protein through the nuclear pore complex into the nucleus. Amongst the members of the importin family, importin subunit alpha-1 and importin subunit alpha-3 have been shown to interact with the NLS of NF-κB p65 and to form a heterodimer with importin subunit beta-1, thereby mediating p65 nuclear translocation [15,17]. VioA time-dependently decreased the total protein level of importin subunit alpha-1 (Fig. 7a), while the total protein levels of importin subunit alpha-3 and importin subunit beta-1 remained unaffected (Fig. 7b-c). An additional effect of vioA different from the inhibition of protein synthesis with regards to importin subunit alpha-1 could be excluded, as up to 16 h of treatment with the natural product had no influence on the mRNA expression of *KPNA2* (Fig. S10a). While the total protein level of importin subunit alpha-3 and importin subunit beta-1 remained stable, vioA even increased the mRNA expression of *KPNA4* and *KPNB1* (Fig. S10b-c). At the same time, the nuclear localization of importin subunit alpha-1 in both non-activated and TNF-activated HUVECs (5–60 min) and of importin subunit beta-1 in TNF-activated (15–30 min) HUVECs was significantly reduced when HUVECs were pretreated with vioA for 16 h, as shown by western blot analysis (Fig. 7d-e). The nuclear accumulation of importin subunit alpha-3 in HUVECs remained unaffected by vioA treatment for 16 h and TNF-activation (Fig. 7f). The purity of the nuclear fraction was ensured

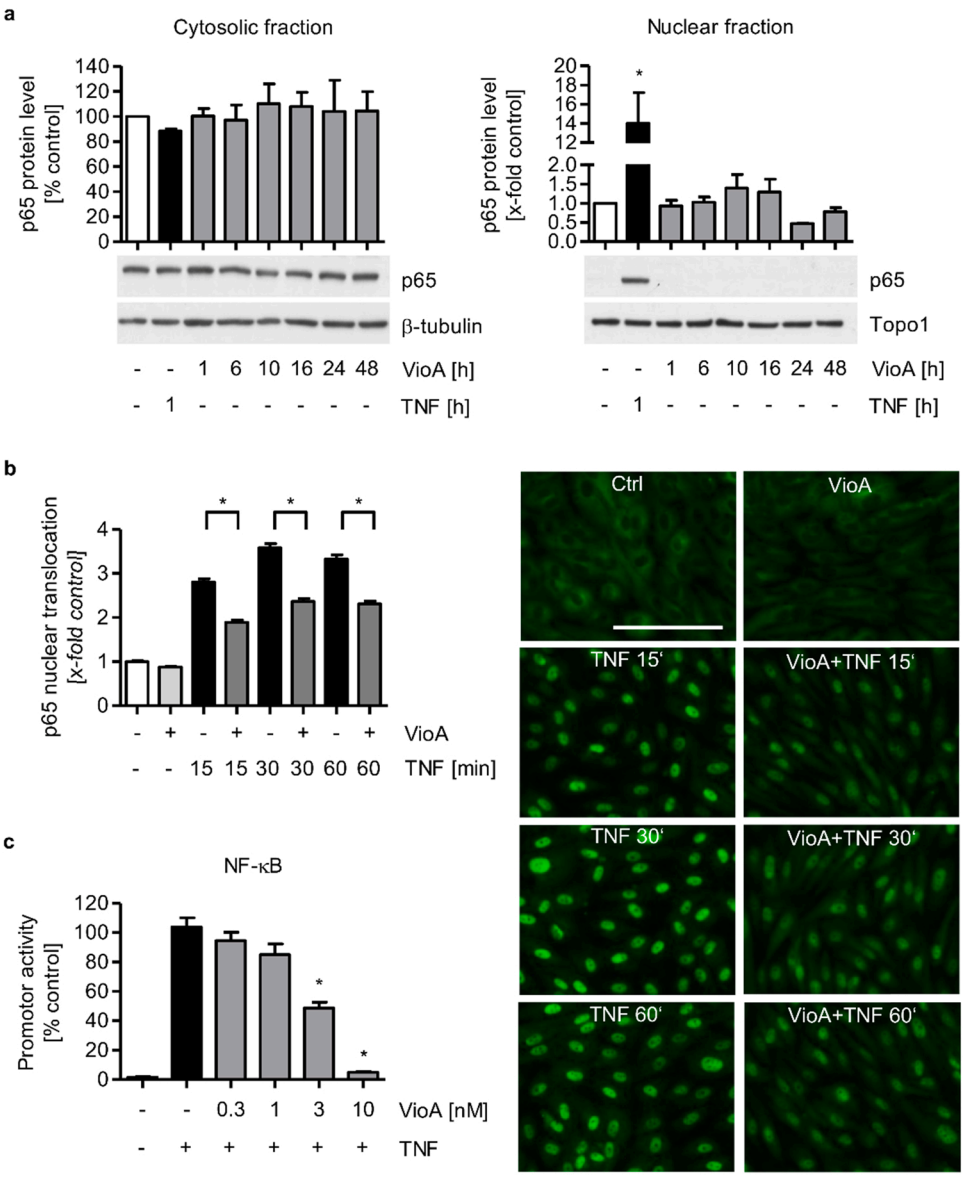

Fig. 6. Vioprolide A reduces TNF-induced p65 translocation and NF-κB promotor activity. a Confluent HUVECs were treated with vioprolide A (10 nM) or TNF (10 ng/ml) as indicated. Cytosolic and nuclear fractions were separated and total protein expression of p65 was analyzed by western blot experiments. One representative blot out of 3 is shown. b Confluent HUVECs were treated with vioprolide A (10 nM) for 16 h followed by TNF (10 ng/ml) activation as indicated. p65 was visualized by immunocytochemistry and fluorescence microscopy. One representative experiment out of 3 is shown. Scale bar, 200 μm. c HUVECs were co-transfected with a vector coding for the NF-κB response element and firefly luciferase and a control vector coding for *Renilla* luciferase. 24 h after transfection, HUVECs were treated with vioprolide A as indicated for 16 h followed by activation with TNF (10 ng/ml) for 6 h. NF-κB-dependent luciferase activity was measured by dual-luciferase reporter gene assay and luminescence measurement. VioA, vioprolide A; Topo1, topoisomerase 1. Data are expressed as mean ± SEM. n = 3 (a, b), n = 4 (c). *P ≤ 0.05 *vs.* negative control (a) or TNF control (b, c).

by western blot analysis of the nuclear and cytosolic markers β-tubulin and topoisomerase I, respectively (Fig. S8b). Note that, although CHX showed similar effects on the total protein level of importin subunit alpha-1/alpha-3/beta-1 (Fig. S11a-c) and potently decreased the nuclear localization of p65 (Fig. S11d), the mRNA expression of *ICAM1* and *SELE* in TNF-activated HUVECs was increased rather than decreased (Fig. S11e). Only the *VCAM1* mRNA expression was reduced (Fig. S11e). These results emphasize that, in contrast to vioA, the CHX-evoked effect on the importin family members and NF-κB p65 is not sufficient for preventing TNF-induced proinflammatory gene expression.

3.8. Knockdown of the vioprolide A target NOP14 evokes reduced leukocyte-endothelial cell interactions caused by a decrease of CAM expression and p65 nuclear translocation

To verify the interaction of vioA with NOP14 in HUVECs, we performed a cellular thermal shift assay (CETSA). In this assay, thermal denaturation and thus protein stability are assessed through heating cells with different temperatures. After cell lysis, denatured and thus aggregated proteins can be removed from the samples through centrifugation and the stable proteins in the supernatant can be analyzed [32].

We investigated the aggregation temperature (T_{agg}) curves of untreated and vioA-treated (300 nM, 1 h) cells by western blot analysis. VioA showed a thermal shift of the NOP14 protein stability from 46.1 °C to 48.2 °C, thus indicating an interaction between the natural product and NOP14 in HUVECs (Fig. 8a). We then strived to investigate a potential anti-inflammatory effect caused by inhibition of NOP14. Therefore, we performed siRNA-mediated knockdown of NOP14 and analyzed its protein level 24 h, 48 h and 72 h after knockdown (Fig. S12). To evaluate the effect of NOP14 knockdown on the leukocyte-endothelial cell interaction we conducted a cell adhesion assay. As demonstrated in Fig. 8b, we found that knockdown of NOP14 significantly reduced the adhesion of fluorescently labeled THP-1 cells to TNF-activated HUVECs, while the basal leukocyte adhesion to non-activated HUVECs was not altered. In addition, the effect of vioA on the adhesion of fluorescently labeled THP-1 cells to the TNF-activated HUVEC monolayer was not further increased. In concert with this, the TNF-induced mRNA expression of *ICAM1* as well as the NF-κB p65 nuclear translocation were significantly decreased in NOP14 knockdown cells, as demonstrated by quantitative real-time PCR (Fig. 8c) and immunofluorescence staining (Fig. 8d). Again, NOP14 knockdown did not further increase the effect of vioA pretreatment (16 h) on *ICAM1* mRNA expression as well as NF-κB

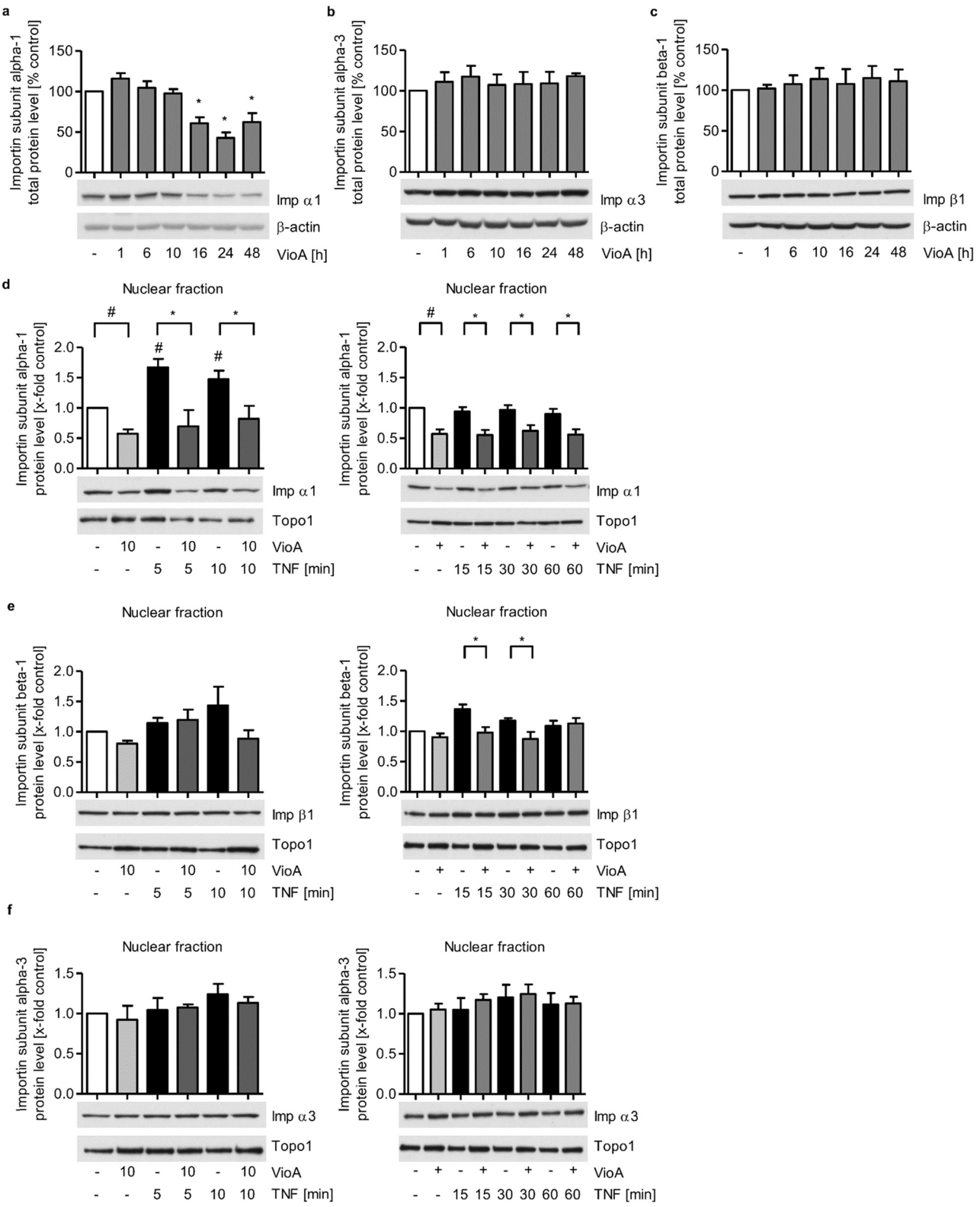

Fig. 7. Vioprolide A reduces importin subunit alpha-1 total protein level and influences importin subunit alpha-1/beta-1 nuclear localization. a-c Confluent HUVECs were treated with vioprolide A (10 nM) as indicated. Total protein levels of importin subunit alpha-1 (a), importin subunit alpha-3 (b) and importin subunit beta-1 (c) were determined by western blot analysis. One representative blot out of 3 is shown. d-f Confluent HUVECs were treated with vioprolide A (10 nM) for 16 h followed by activation with TNF (10 ng/ml) as indicated. The nuclear fractions were separated and total nuclear protein expression of importin subunit alpha-1 (d), importin subunit beta-1 (e) and importin subunit alpha-3 (f) was determined by western blot analysis. One representative blot out of 3 is shown. VioA, vioprolide A; Imp, importin; Topo1, topoisomerase 1. Data are expressed as mean ± SEM. n = 3. *P ≤ 0.05 *vs.* negative control (a-c) or TNF control (d-f). #P ≤ 0.05 *vs.* negative control (d-f).

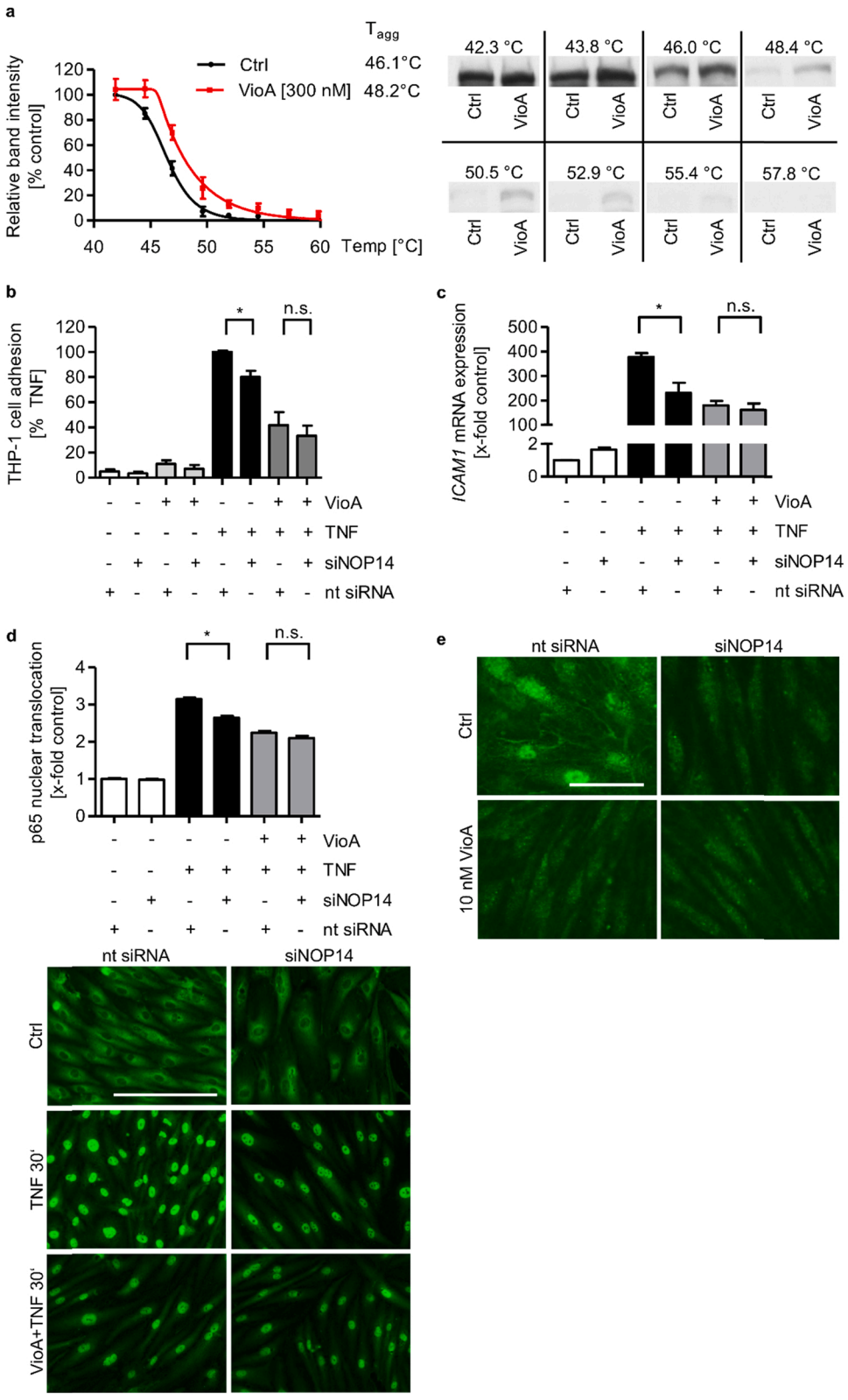

Fig. 8. NOP14 knockdown influences TNF-activated inflammatory processes in HUVECs. a Confluent HUVECs were treated with 300 nM vioprolide A for 1 h or left untreated. Cells were exposed to increasing temperatures between 42.3 and 57.8 °C and lysed by repeated freeze-thaw cycles in liquid nitrogen. Thermal aggregation curves of NOP14 were analyzed by western blot. One representative blot out of 4 is shown. b-e Subconfluent cells were transfected with siRNA against NOP14 (siNOP14, 60 nM) or non-targeting siRNA (nt siRNA, 60 nM) as control using GeneTrans II Transfection Reagent. 30 h after transfection, HUVECs were treated with 10 nM vioprolide A for 16 h. b HUVECs were activated with TNF (10 ng/ml) for 6 h and fluorescence-labeled THP-1 cells were allowed to adhere to the HUVEC monolayer for 5 min. The amount of adhered THP-1 was detected by fluorescence measurement. c HUVECs were activated with TNF (10 ng/ml) for 4 h. The mRNA expression of *ICAM1* was analyzed by quantitative PCR. d HUVECs were activated with TNF (10 ng/ml) for 30 min p65 was visualized by immunocytochemistry and fluorescence microscopy. One representative experiment out of 3 is shown. Scale bar, 200 μm. e Importin subunit alpha-1 was visualized by immunocytochemistry and fluorescence microscopy. One representative experiment out of 3 is shown. Scale bar, 50 μm. T_{agg}, aggregation temperature; VioA, vioprolide A. Data are expressed as mean ± SEM. n = 4 (a), n = 5 (b), n = 3 (c-e). *P ≤ 0.05 *vs.* TNF control.

p65 nuclear translocation in TNF-activated HUVECs. Immunofluorescence staining of importin subunit alpha-1 further revealed that NOP14 knockdown decreased the fluorescence intensity and thus cellular importin subunit alpha-1 protein level equally strong compared to 16 h vioA (10 nM) treatment (Fig. 8e). These results clearly underline the involvement of NOP14 in inflammatory processes in the endothelium and demonstrate that the anti-inflammatory actions of vioA are, at least in part, evoked by inhibition of NOP14.

4. Discussion

In this study, we focused on the anti-inflammatory actions of the

natural product vioA *in vivo* and *in vitro*. VioA exerted strong anti-inflammatory effects *in vivo* by reducing the laser lesion area infiltration of microglia and macrophages in a murine CNV model and by lowering the interaction between leukocytes and the vascular endothelium as observed by intravital microscopy of the murine cremaster muscle. Although the rolling motion of the leukocytes was not impaired by vioA, their firm adhesion to and transmigration through the vascular endothelium was strongly reduced. I*n vitro* models further showed that vioA significantly decreased both the leukocyte adhesion to and transmigration through TNF-activated endothelial cells due to an inhibition of the cell surface and total protein expression of CAMs. Although vioA also potently reduced the TNF-induced mRNA expression of the coding genes for ICAM-1, VCAM-1 (4 h and 6 h TNF) and E-selectin (2 h and 4 h TNF), the effect on the protein levels was stronger compared to the reduction of the mRNA levels. This led to the hypothesis that the anti-inflammatory action of vioA is not only attributed to the impairment of inflammatory gene expression but also to the prevention of proper mRNA translation into functional proteins. This notion was furthermore strengthened by recently published data demonstrating that vioA targets the nucleolar protein 14 (NOP14), which is involved in the ribosomal biogenesis [3]. By using a protein translation assay, which monitors the incorporation of OPP into newly synthesized proteins, we verified that vioA reduced the *de novo* protein synthesis also in endothelial cells. These results indicate that the protein level of CAMs upon vioA treatment is reduced through a dual mechanism. On the one hand, vioA impairs the NF-κB signaling pathway through reducing the p65 nuclear translocation and NF-κB promotor activity. This explains the reduction of TNF-induced CAM mRNA expression. On the other hand, vioA acts as inhibitor of general *de novo* protein synthesis. Thus, although a reduced amount of CAM mRNA is still expressed in vioA-treated endothelial cells, protein synthesis inhibition prevents its translation into protein.

Interestingly, over the last years, various inhibitors of mRNA translation have been identified to exert anti-inflammatory actions. The bacteria-derived mycotrienin II and cytotrienin A were shown to reduce the TNF-induced ICAM-1 expression in human lung carcinoma cells due to a ribotoxic stress response leading to ectodomain shedding of the TNFR1 [35,36]. The plant-derived alkaloid narciclasine was found to act anti-inflammatorily in HUVECs by reducing the TNFR1 protein level, thereby inhibiting the downstream NF-κB signaling cascade [34]. Also, derivatives of the *Aglaia* flavagline rocaglamide were shown to influence the NF-κB activity by prohibiting the phosphorylation and subsequent degradation of IκBα in T cells [37]. The NF-κB signaling cascade, which can be activated *via* the binding of TNF to the TNFR1, represents one of the most important inflammatory pathways in endothelial cells and its inhibition has been shown to be efficient in the treatment of chronic inflammation [38]. Thus, we further investigated a potential connection between the anti-inflammatory actions of vioA and the NF-κB signaling pathway. In concert with the effects of narciclasine, vioA potently downregulated the protein level of the TNFR1, while the *TNFRSF1A* mRNA level was time-dependently increased. Accordingly, the phosphorylation and thus activation of the downstream kinases TAK and IKK in TNF-activated HUVECs was significantly reduced by vioA. Nevertheless, in contrast to narciclasine, vioA did not rescue the IκBα protein level in TNF-treated endothelial cells but instead already decreased the total protein level of IκBα in the absence of TNF. Again, vioA simultansously upregulated the *NFKBIA* mRNA level, which is most likely attributed to a feedback mechanism of the cells towards the reduction of *de novo* protein synthesis. IκBα showed a longer half-live upon CHX treatment compared to the TNFR1. This can be attributed to the interaction of IκBα with cytosolic NF-κB subunits, which leads to a stabilization of the protein and explains why the protein level decreases more slowly upon inhibition of protein synthesis compared to the protein level of the TNFR1 [39]. Interestingly, although protein synthesis in HUVECs after vioA treatment was gradually restored within 24–48 h, the IκBα protein level showed no recovery. It is important to mention that in this study we focused on the anti-inflammatory effect of vioA and thus investigated the influence of the natural product on the TNF-induced NF-κB signaling pathway and on general protein synthesis. However, other intracellular signaling pathways can interfere with IκBα stability and degradation, too. As an example, it has been shown that increased Akt (protein kinase B) activation evokes the phosphorylation of IKK which in the following leads to the phosphorylation and degradation of IκBα [40]. As the strongest influence of vioA on the TNFR1 was observed after 16 h, we only investigated the activation of downstream kinases (TAK, IKK) after 16 h of vioA treatment and only using TNF as activator. Thus, we cannot draw any conclusions on how these kinases are influenced after longer vioA treatment periods of 24 h and 48 h or using different activators. In contrast to IκBα and the TNFR1, the NF-κB p65 protein level remained unaffected in HUVECs upon treatment with vioA, which indicates a long half-life period of the protein. In addition, the TNF-induced NF-κB p65 nuclear translocation as well as the NF-κB promotor activity were strongly impaired by vioA.

Importins are carrier proteins that bind the NLS of NF-κB p65, thereby shuttling the protein through the pore complexes into the nucleus. In many chronic pathologies, including rheumatoid arthritis, atherosclerosis, or inflammatory bowel diseases (IBD) and even cancer, members of the importin α- and β-family are crucially involved [41–44]. An upregulation of importin subunit alpha-1 for example has been observed in patients with rheumatoid arthritis compared to healthy control patients [45]. These data suggest that dysregulation of importins is an important aspect of chronic inflammatory diseases. Hence, addressing deregulated importins represents a promising treatment possibility [46]. We demonstrated that vioA evoked a time-dependent reduction of the importin subunit alpha-1 protein level accompanied by an inhibition of the importin subunit alpha-1 and importin subunit beta-1 nuclear localization in TNF-activated vascular endothelial cells. These results show that, although both vioA and narciclasine act as inhibitors of eukaryotic protein synthesis, the natural products influence the expression of, at least in part, differing proteins, which leads to unique modes of action. This observation is furthermore strengthened by the finding that, although also CHX reduced the protein expression of importin subunit alpha-1, the protein synthesis inhibitor increased rather than decreased the mRNA expression of the CAM encoding genes *ICAM1* and *SELE* in TNF-activated HUVECs.

As shown previously, vioA interacts with the nucleolar protein NOP14 in Jurkat cells. Through performing a cellular thermal shift assay, we could verify that vioA also binds to NOP14 in HUVECs. Although various studies underline the involvement of NOP14 in angiogenic processes in cancer, nothing is known about the general involvement of NOP14 in inflammatory actions [4–7]. To elucidate this important point, we performed siRNA-mediated knockdown of NOP14 in HUVECs. We found that NOP14 knockdown significantly reduced the adhesion of leukocytes to TNF-activated endothelial cells. In concert with the action of vioA, NOP14 knockdown also reduced the TNF-induced *ICAM1* mRNA expression, p65 nuclear translocation and importin subunit alpha-1 protein level in HUVECs. Importantly, the effects of vioA were not further increased in combination with NOP14 knockdown. NOP14 knockdown alone, however, had slightly less potent effects in the conducted experiments compared to vioA. This could be explained by the fact that siRNA-mediated knockdown of NOP14 only reduced its protein level to ~40% of control level. Thus, the observed effects cannot be equated to a complete knockout of the protein. In total, we propose that the anti-inflammatory action of vioA is, at least in part, attributed to its interaction with NOP14. VioA is the first ever mentioned natural product that interacts with the NOP14-associated pathway of ribosomal biogenesis. The protein NOP14 again has been shown to be differentially expressed in various cell types [4–7]. This renders both vioA as drug lead as well as NOP14 as cellular target highly unique. Moreover, our data indicate that NOP14 is not only involved in angiogenic events but is also important for inflammatory processes in vascular endothelial cells.

Taken together, we could demonstrate for the first time that vioA

inhibits TNF-induced inflammatory processes in endothelial cells and reduces the leukocyte-endothelial cell interaction. To our knowledge, this is also the first time that the anti-inflammatory action of a protein synthesis inhibitor could be linked to the impairment of carrier proteins of the importin family. We conclude that vioA is a highly potent and unique natural product that provides promising effects on inflammation-related processes in the vascular endothelium by reducing leukocyte-endothelial cell interactions and targeting the importin family of carrier proteins without exerting cytotoxic effects. Especially by targeting NOP14 and thus *de novo* protein synthesis in a unique way, vioA represents a promising drug lead for the selective treatment of chronic inflammatory diseases that are associated with deregulated importin family member or NOP14 expression, which warrants further in-depth research.

Funding

This work was supported by the Hessisches Ministerium für Wissenschaft und Kunst, Landesoffensive zur Entwicklung wissenschaftlich-ökonomischer Exzellenz (LOEWE) Center "Translational Biodiversity Genomics" (TBG), Germany.

CRediT authorship contribution statement

Luisa D. Burgers: Conceptualization, Methodology, Formal analysis, Investigation, Writing – original draft, Visualization. **Betty Luong**: Investigation. **Yanfen Li**: Investigation, Formal analysis. **Matthias P. Fabritius**: Investigation, Formal analysis, Writing – review & editing. **Stylianos Michalakis**: Methodology, Investigation, Formal analysis, Writing – review & editing. **Christoph A. Reichel**: Methodology, Investigation, Formal analysis, Resources, Writing – review & editing. **Rolf Müller**: Resources, Funding acquisition. **Robert Fürst**: Conceptualization, Methodology, Validation, Resources, Writing – review & editing, Supervision, Project administration, Funding acquisition.

Ethics approval

All experimental procedures were conducted in compliance with the German legislation for the protection of animals. Animal experiments were approved by the Government of Upper Bavaria under the reference numbers ROB-55.2–2532-Vet 02–15–50 (CNV model; 08–10–2015), and ROB-55.2Vet-2532. Vet_02–17–68 (intravital microscopy; 01–03–2018).

Conflict of interest statement

The authors declare that they have no known competing financial interests or personal relationships that could have appeared to influence the work reported in this paper.

Acknowledgment

We acknowledge the help of Daniel Sauer in isolating vioprolide A and of Dr. Ilse Zündorf for her help and support in creating the graphical abstract. For initial support in CETSA experiments, we would like to thank Dr. Iris Bischoff-Kont.

Appendix A. Supporting information

Supplementary data associated with this article can be found in the online version at doi:10.1016/j.biopha.2021.112255.

References

[1] D. Schummer, E. Forche, V. Wray, T. Domke, et al., Antibiotics from gliding bacteria.76. Vioprolides: new antifungal and cytotoxic peptolides from Cystobacter violaceus, Liebigs Ann. 6 (1996) 971–978.
[2] D. Chauhan, E. Bartok, M.M. Gaidt, F.J. Bock, J. Herrmann, J.M. Seeger, P. Broz, R. Beckmann, H. Kashkar, S. Tait, R. Müller, V. Hornung, BAX/BAK-induced apoptosis results in caspase-8-dependent IL-1beta maturation in macrophages, Cell Rep. 25 (9) (2018) 2354–2368, https://doi.org/10.1016/j.celrep.2018.10.087.
[3] V.C. Kirsch, C. Orgler, S. Braig, I. Jeremias, D. Auerbach, R. Müller, A.M. Vollmar, S.A. Sieber, The cytotoxic natural product vioprolide A targets nucleolar protein 14, which is essential for ribosome biogenesis, Angew. Chem. Int. Ed. Engl. 59 (4) (2020) 1595–1600, https://doi.org/10.1002/anie.201911158.
[4] Y. Du, Z. Liu, L. You, P. Hou, X. Ren, T. Jiao, W. Zhao, Z. Li, H. Shu, C. Liu, Y. Zhao, Pancreatic cancer progression relies upon mutant p53-induced oncogenic signaling mediated by NOP14, Cancer Res. 77 (10) (2017) 2661–2673, https://doi.org/10.1158/0008-5472.CAN-16-2339.
[5] J. Li, R. Fang, J. Wang, L. Deng, NOP14 inhibits melanoma proliferation and metastasis by regulating Wnt/β-catenin signaling pathway, Braz. J. Med. Biol. Res. 52 (1) (2018), 7952, https://doi.org/10.1590/1414-431×20187952.
[6] Y. Ying, J. Li, H. Xie, H. Yan, K. Jin, L. He, X. Ma, J. Wu, X. Xu, J. Fang, X. Wang, X. Zheng, B. Liu, L. Xie, CCND1, NOP14 and DNMT3B are involved in miR-502-5p-mediated inhibition of cell migration and proliferation in bladder cancer, Cell Prolif. 53 (2) (2020), 12751, https://doi.org/10.1111/cpr.12751.
[7] B. Zhou, Q. Wu, G. Chen, T.P. Zhang, Y.P. Zhao, NOP14 promotes proliferation and metastasis of pancreatic cancer cells, Cancer Lett. 322 (2) (2012) 195–203, https://doi.org/10.1016/j.canlet.2012.03.010.
[8] S. Nourshargh, R. Alon, Leukocyte migration into inflamed tissues, Immunity 41 (5) (2014) 694–707, https://doi.org/10.1016/j.immuni.2014.10.008.
[9] S. Baratchi, K. Khoshmanesh, O.L. Woodman, S. Potocnik, K. Peter, P. McIntyre, Molecular sensors of blood flow in endothelial cells, Trends Mol. Med. 23 (9) (2017) 850–868, https://doi.org/10.1016/j.molmed.2017.07.007.
[10] G. Bazzoni, E. Dejana, Endothelial cell-to-cell junctions: molecular organization and role in vascular homeostasis, Physiol. Rev. 84 (3) (2004) 869–901, https://doi.org/10.1152/physrev.00035.2003.
[11] R.D. Minshall, A.B. Malik, Transport across the endothelium: regulation of endothelial permeability, Handb. Exp. Pharmacol. 176 Pt 1 (2006) 107–144, https://doi.org/10.1007/3-540-32967-6_4.
[12] L. Chen, H. Deng, H. Cui, J. Fang, Z. Zuo, J. Deng, Y. Li, X. Wang, L. Zhao, Inflammatory responses and inflammation-associated diseases in organs, Oncotarget 9 (6) (2018) 7204–7218, https://doi.org/10.18632/oncotarget.23208.
[13] M.S. Hayden, S. Ghosh, Regulation of NF-kappaB by TNF family cytokines, Semin. Immunol. 26 (3) (2014) 253–266, https://doi.org/10.1016/j.smim.2014.05.004.
[14] A. Lange, R.E. Mills, C.J. Lange, M. Stewart, S.E. Devine, A.H. Corbett, Classical nuclear localization signals: definition, function, and interaction with importin alpha, J. Biol. Chem. 282 (8) (2007) 5101–5105, https://doi.org/10.1074/jbc.R600026200.
[15] Y. Cai, Y. Shen, L. Gao, M. Chen, M. Xiao, Z. Huang, D. Zhang, Karyopherin alpha 2 promotes the inflammatory response in rat pancreatic acinar cells via facilitating NF-kappab activation, Dig. Dis. Sci. 61 (3) (2016) 747–757, https://doi.org/10.1007/s10620-015-3948-6.
[16] R. Fagerlund, L. Kinnunen, M. Köhler, I. Julkunen, K. Melén, NF-{kappa}B is transported into the nucleus by importin {alpha}3 and importin {alpha}4, J. Biol. Chem. 280 (16) (2005) 15942–15951, https://doi.org/10.1074/jbc.M500814200.
[17] P. Liang, H. Zhang, G. Wang, S. Li, S. Cong, Y. Luo, B. Zhang, KPNB1, XPO7 and IPO8 mediate the translocation ofNF-kappaB/p65 into the nucleus, Traffic 14 (11) (2013) 1132–1143, https://doi.org/10.1111/tra.12097.
[18] R. Tao, X. Xu, C. Sun, Y. Wang, S. Wang, Z. Liu, L. Zhai, H. Cheng, M. Xiao, D. Zhang, KPNA2 interacts with P65 to modulate catabolic events in osteoarthritis, Exp. Mol. Pathol. 99 (2) (2015) 245–252, https://doi.org/10.1016/j.yexmp.2015.07.007.
[19] F. Yang, S. Li, Y. Cheng, J. Li, X. Han, Karyopherin α 2 promotes proliferation, migration and invasion through activating NF-κB/p65 signaling pathways in melanoma cells, Life Sci. 252 (2020), 117611, https://doi.org/10.1016/j.lfs.2020.117611.
[20] Y. Zhuo, Z. Guo, T. Ba, C. Zhang, L. He, C. Zeng, H. Dai, African swine fever virus MGF360–12 L inhibits type I interferon production by blocking the interaction of importin alpha and NF-kappaB signaling pathway, Virol. Sin. 36 (2) (2021) 176–186, https://doi.org/10.1007/s12250-020-00304-4.
[21] T. Liu, L. Zhang, D. Joo, S.C. Sun, NF-κB signaling in inflammation, Signal Transduct. Target. Ther. 2 (2017) 2, https://doi.org/10.1038/sigtrans.2017.23.
[22] C.N. Serhan, N. Chiang, J. Dalli, B.D. Levy, Lipid mediators in the resolution of inflammation, Cold Spring Harb. Perspect. Biol. 7 (2) (2014), 016311, https://doi.org/10.1101/cshperspect.a016311.
[23] Y.Y. Li, T.M. Zollner, M.P. Schon, Targeting leukocyte recruitment in the treatment of psoriasis, Clin. Dermatol. 26 (5) (2008) 527–538, https://doi.org/10.1016/j.clindermatol.2007.11.002.
[24] R. Bordy, P. Totoson, C. Prati, C. Marie, D. Wendling, C. Demougeot, Microvascular endothelial dysfunction in rheumatoid arthritis, Nat. Rev. Rheumatol. 14 (7) (2018) 404–420, https://doi.org/10.1038/s41584-018-0022-8.
[25] F.K. Swirski, M. Nahrendorf, Leukocyte behavior in atherosclerosis, myocardial infarction, and heart failure, Science 339 (6116) (2013) 161–166, https://doi.org/10.1126/science.1230719.
[26] E.A. Jaffe, R.L. Nachman, C.G. Becker, C.R. Minick, Culture of human endothelial cells derived from umbilical veins. Identification by morphologic and immunologic

criteria, J. Clin. Invest. 52 (11) (1973) 2745–2756, https://doi.org/10.1172/JCI107470.
[27] A. Boyum, Isolation of lymphocytes, granulocytes and macrophages, Scand. J. Immunol. Suppl 5 (1976) 9–15.
[28] V. Lambert, J. Lecomte, S. Hansen, S. Blacher, M.L. Gonzalez, I. Struman, N. E. Sounni, E. Rozet, P. de Tullio, J.M. Foidart, J.M. Rakic, A. Noel, Laser-induced choroidal neovascularization model to study age-related macular degeneration in mice, Nat. Protoc. 8 (11) (2013) 2197–2211, https://doi.org/10.1038/nprot.2013.135.
[29] S. Baez, An open cremaster muscle preparation for the study of blood vessels by in vivo microscopy, Microvasc. Res. 5 (3) (1973) 384–394, https://doi.org/10.1016/0026-2862(73)90054-x.
[30] T.R. Mempel, C. Moser, J. Hutter, W.M. Kuebler, F. Krombach, Visualization of leukocyte transendothelial and interstitial migration using reflected light oblique transillumination in intravital video microscopy, J. Vasc. Res. 40 (5) (2003) 435–441, https://doi.org/10.1159/000073902.
[31] I. Nicoletti, G. Migliorati, M.C. Pagliacci, F. Grignani, C. Riccardi, A rapid and simple method for measuring thymocyte apoptosis by propidium iodide staining and flow cytometry, J. Immunol. Methods 139 (2) (1991) 271–279, https://doi.org/10.1016/0022-1759(91)90198-o.
[32] R. Jafari, H. Almqvist, H. Axelsson, M. Ignatushchenko, T. Lundbäck, P. Nordlund, D. Martinez Molina, The cellular thermal shift assay for evaluating drug target interactions in cells, Nat. Protoc. 9 (9) (2014) 2100–2122, https://doi.org/10.1038/nprot.2014.138.
[33] U. Utans, R.J. Arceci, Y. Yamashita, M.E. Russell, Cloning and characterization of allograft inflammatory factor-1: a novel macrophage factor identified in rat cardiac allografts with chronic rejection, J. Clin. Invest. 95 (6) (1995) 2954–2962, https://doi.org/10.1172/JCI118003.
[34] A. Stark, R. Schwenk, G. Wack, G. Zuchtriegel, M.G. Hatemler, J. Bräutigam, A. Schmidtko, C.A. Reichel, I. Bischoff, R. Fürst, Narciclasine exerts anti-inflammatory actions by blocking leukocyte-endothelial cell interactions and down-regulation of the endothelial TNF receptor 1, Faseb J. 33 (8) (2019) 8771–8781, https://doi.org/10.1096/fj.201802440R.
[35] Y. Yamada, S. Taketani, H. Osada, T. Kataoka, Cytotrienin A, a translation inhibitor that induces ectodomain shedding of TNF receptor 1 via activation of ERK and p38 MAP kinase, Eur. J. Pharmacol. 667 (1–3) (2011) 113–119, https://doi.org/10.1016/j.ejphar.2011.05.072.
[36] Y. Yamada, E. Tashiro, S. Taketani, M. Imoto, T. Kataoka, Mycotrienin II, a translation inhibitor that prevents ICAM-1 expression induced by pro-inflammatory cytokines, J. Antibiot. (Tokyo). 64 (5) (2011) 361–366, https://doi.org/10.1038/ja.2011.23.
[37] B. Baumann, F. Bohnenstengel, D. Siegmund, H. Wajant, C. Weber, I. Herr, K. M. Debatin, P. Proksch, T. Wirth, Rocaglamide derivatives are potent inhibitors of NF-kappa B activation in T-cells, J. Biol. Chem. 277 (47) (2002) 44791–44800, https://doi.org/10.1074/jbc.M208003200.
[38] S. Kempe, H. Kestler, A. Lasar, T. Wirth, NF-kappaB controls the global pro-inflammatory response in endothelial cells: evidence for the regulation of a pro-atherogenic program, Nucleic Acids Res. 33 (16) (2005) 5308–5319, https://doi.org/10.1093/nar/gki836.
[39] E. Mathes, E.L. O'Dea, A. Hoffmann, G. Ghosh, NF-kappaB dictates the degradation pathway of IkappaBalpha, EMBO J. 27 (9) (2008) 1357–1367, https://doi.org/10.1038/emboj.2008.73.
[40] D. Bai, L. Ueno, P.K. Vogt, Akt-mediated regulation of NFkappaB and the essentialness of NFkappaB for the oncogenicity of PI3K and Akt, Int. J. Cancer 125 (12) (2009) 2863–2870, https://doi.org/10.1002/ijc.24748.
[41] A. Leonard, A. Rahman, F. Fazal, Importins alpha and beta signaling mediates endothelial cell inflammation and barrier disruption, Cell. Signal. 44 (2018) 103–117, https://doi.org/10.1016/j.cellsig.2018.01.011.
[42] S.M. Rachidi, T. Qin, S. Sun, W.J. Zheng, Z. Li, Molecular profiling of multiple human cancers defines an inflammatory cancer-associated molecular pattern and uncovers KPNA2 as a uniform poor prognostic cancer marker, PLoS One 8 (3) (2013), 57911, https://doi.org/10.1371/journal.pone.0057911.
[43] X. Sun, S. He, A. Wara, B. Icli, E. Shvartz, Y. Tesmenitsky, N. Belkin, D. Li, T. S. Blackwell, G.K. Sukhova, K. Croce, M.W. Feinberg, Systemic delivery of microRNA-181b inhibits nuclear factor-kappaB activation, vascular inflammation, and atherosclerosis in apolipoprotein E-deficient mice, Circ. Res. 114 (1) (2014) 32–40, https://doi.org/10.1161/CIRCRESAHA.113.302089.
[44] X. Sun, B. Icli, A.K. Wara, N. Belkin, S. He, L. Kobzik, G.M. Hunninghake, M. P. Vera, R. MICU, T.S. Blackwell, R.M. Baron, M.W. Feinberg, MicroRNA-181b regulates NF-kappaB-mediated vascular inflammation, J. Clin. Invest. 122 (6) (2012) 1973–1990, https://doi.org/10.1172/JCI61495.
[45] Z. Liu, D. Zhang, C. Sun, R. Tao, X. Xu, L. Xu, H. Cheng, M. Xiao, Y. Wang, KPNA2 contributes to the inflammatory processes in synovial tissue of patients with rheumatoid arthritis and SW982 cells, Inflammation 38 (6) (2015) 2224–2234, https://doi.org/10.1007/s10753-015-0205-2.
[46] A. Mahipal, M. Malafa, Importins and exportins as therapeutic targets in cancer, Pharmacol. Ther. 164 (2016) 135–143, https://doi.org/10.1016/j.pharmthera.2016.03.020.